Fabrication and Interfacial Property Analysis of Electroless-Deposited Nanostructures for Imprinting Mold

July, 2013

Cheng Ping LIN

Fabrication and Interfacial Property Analysis of Electroless-Deposited Nanostructures for Imprinting Mold

July, 2013

Waseda University

Graduate School of Advanced Science and Engineering

Major in Applied Chemistry

Research on Interfacial Electrochemistry

Cheng Ping LIN

Contents

Chapter 1 Introduction

1.1. Nanoimprint lithography 2
1.2. Electroless deposition 9
1.3. Self assembled monolayer 12
1.4. Nanoindentation 18
1.5. Nanoindentation analysis for hardness 21
1.6. Purpose of this thesis 25
References 26

Chapter 2 Initial catalyzation analysis of SAM modified SiO_2 surface for electroless NiP imprinting mold fabrication

2.1 Introduction 32
2.2 Experimental Methods 34
2.3 Results and Discussion
2.3.1 The surface morphology of a flat SiO_2 substrate after initial catalyzation 38
2.3.2 Pd catalyst coverage on a flat SiO_2 substrate after initial catalyzation 40
2.3.3 The surface morphology of electroless deposited NiP on a flat SiO_2 substrate 43
2.3.4 The surface morphology of electroless deposited NiP on a trench-patterned master mold 45
2.3.5 Adhesion strength between electroless deposited NiP and SiO_2 surface 46
2.3.6 Replication of master mold 48
2.3.7 Sub-20 nm scale replication ability to master mold 50
2.3.8 Conditions of self assembled monolayer after detachment 51
2.3.9 Effect of self assembled monolayer on the adhesion strength 54
2.4 Conclusion 56
References 57

Chapter 3 Surface analysis of UV-treated cyclo olefin polymer for electroless NiP imprinting mold fabrication

3.1 Introduction 60
3.2 Experimental Methods 62
3.3 Results and Discussion
3.3.1 APTES formation on UV-irradiation-treated COP surface 65
3.3.2 Optimization of UV irradiation treatment time 67
3.3.3 Replicate mold 70
3.4 Conclusion 71
Appendix 72
References 73

Chapter 4 Nanoindentation analysis for mechanical properties of electroless NiP imprinting mold

4.1 Introduction 76
4.2 Experimental Methods 78
4.3 Results and Discussion
4.3.1 The crystal property of deposited NiP 82
4.3.2 The surface morphology of as-deposited NiP and detached NiP 83
4.3.3 The hardness of as-deposited NiP and detached NiP 85
4.3.4 Initial deposition of NiP in various sizes nanopattern of master mold 87
4.3.5 Nanoindentation analysis for mechanical property of various sizes NiP nanopattern 89
4.4 Conclusion 92
References 93

Chapter 5 General Conclusion 96

List of Achievements 102

Acknowledgement 106

Chapter 1

Introduction

1. 1. Nanoimprint lithography

General principle of nanoimprint lithography

Nanoimprint lithography (NIL) process, which was proposed from Chou et al. in 1995 [1], is an effective process for 3D nanopatterned fabrication. The general principle of nanoimprint process is shown by Fig. 1. 1. 1. A hard mold with 3D nanopatterned surface is physically pressed on a polymeric material coated substrate at a specific temperature and pressure for nanopattern transfer on the polymeric material. In general, a thin residual layer of polymeric material is intentionally left between the mold and polymeric material coated substrate for preventing the nanopattern of mold directly contact the substrate, and protects the delicate nanopatterns of mold. The mold is then detached from the substrate. The anisotropic etching process is typically used to remove the residual layer for completing nanopattern transfer.

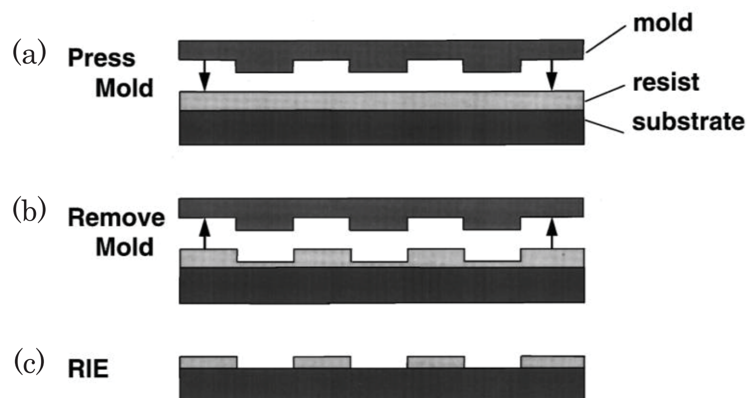

Fig. 1. 1. 1. Schematic illustrations of NIL process: (a) to press a mold on a polymeric material coated substrate, (b) mold detachment, (c) to remove residual polymeric material using anisotropic etching process for completing nanopattern transfer [2].

Merits of nanoimprint lithography

NIL is an attractive and widely studied technology because of it can fabricate sub-10 nm nanopatterns with ultrahigh resolution. Fig. 1. 1. 2a show the scanning electron microscope (SEM) image of a SiO_2 imprinting mold with 10 nm diameter pillar array, and 10 nm diameter holes are observed on the imprinted poly(methyl methacrylate) (PMMA) (Fig. 1. 1. 2b). Furthermore, the parallel imprinting processes and simple equipment set-up of NIL make the high throughput and low cost processes can be achieved.

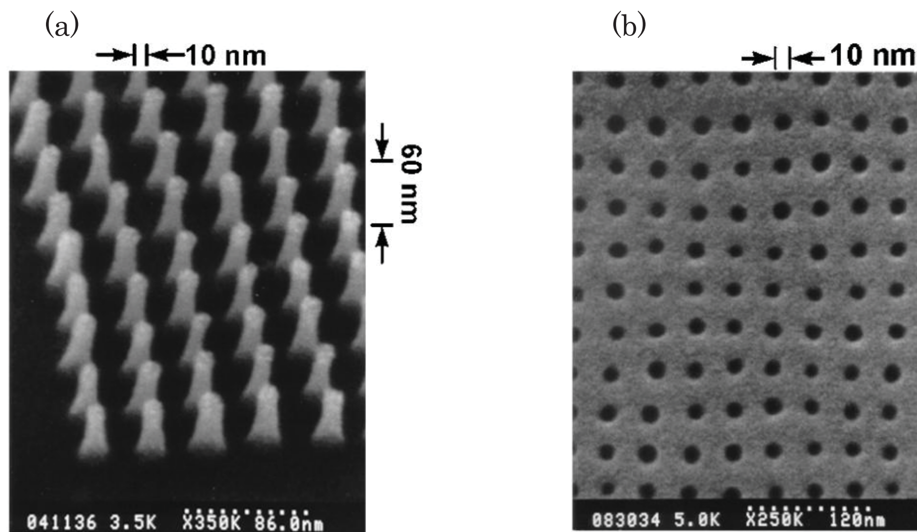

Fig. 1. 1. 2. (a) SEM images of a SiO_2 mold with 10 nm diameter pillars, and (b) the imprinted PMMA which has 10 nm diameter holes [3].

Applications of nanoimprint lithography

Because of the merits described above, NIL is expected to be the next-generation fabrication process of electronic devices [4-5], optical elements [6-8], biotechnology [9-10], and magnetic storage devices [11-14], which require 3D nanostructured surfaces.

NIL for electronic devices

Chou et al. [4] successfully fabricated 60nm channel metal oxide semiconductor field effect transistors (MOSFETs) by using NIL process (Fig. 1. 1. 3), and demonstrated

that the NIL processes with enough overlay accuracy (500 nm in both X and Y directions) in manufacturing of electronic devices.

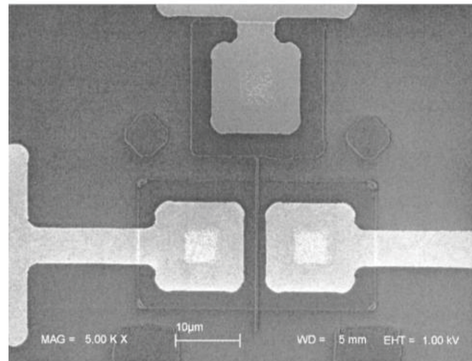

Fig. 1. 1. 3. The SEM image of a 60 nm channel length MOSFET fabricated by NIL process [4].

NIL for optical elements

Guo et al. [6] fabricated pixelated organic polymer light-emitting devices (OPLED) by using NIL process (Fig. 1. 1. 4) and demonstrated that the NIL fabricated OPLED pixels possess comparable optoelectronic characterization with OPLED pixels formed by other fabrication methods.

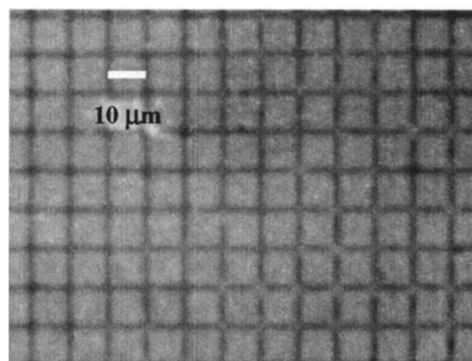

Fig. 1. 1. 4. An optical micrograph of lighted OPLED arrays fabricated by NIL process [6].

NIL for biotechnology

Pang et al. [10] applied NIL process to form nanostructures on a tissue-culture polystyrene (TCPS) substrate, and smooth muscle cells (SMCs) were cultured on the patterned TCPS substrate. The cell elongation and alignment were observed on the patterned TCPS substrate (Fig. 1. 1. 5b), indicating that the cell morphology is affected by the surface structure, which can be easily formed by NIL process.

(a) (b)

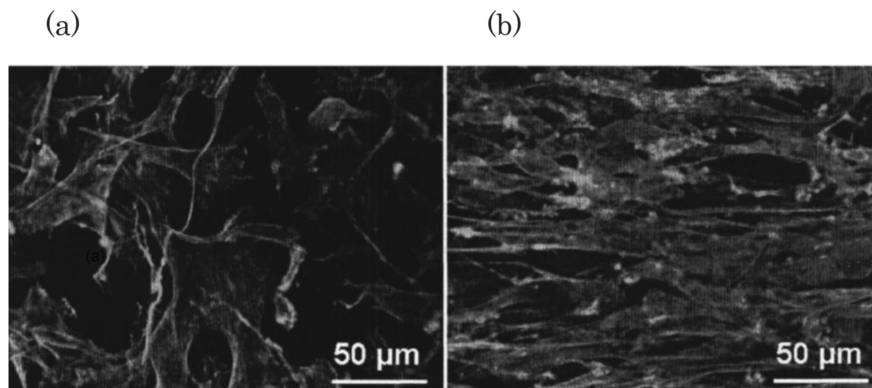

Fig. 1. 1. 5. Fluorescence images of SMCs on (a) unpatterned or (b) patterned TCPS substrate [10].

NIL for magnetic storage devices

Chou et al. [12] used NIL process, electrodeposition, and chemical mechanical polishing to fabricate large area quantized magnetic disks (QMDs). A Ni pillar (70 nm diameter) was formed, and clear magnetic pole was observed at each pillar position, indicating each Ni pillar is a single magnetic domain (Fig. 1. 1. 6).

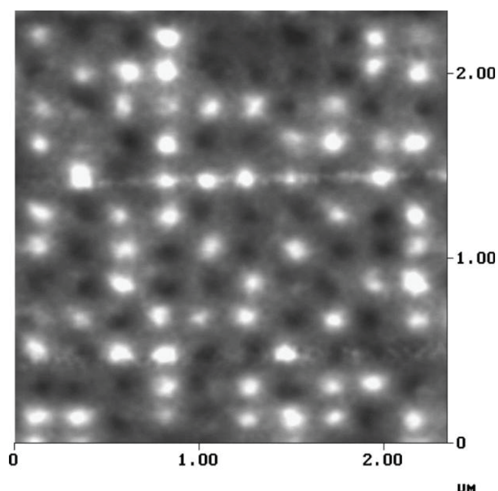

Fig. 1. 1. 6. A magnetic force microscopy image of perpendicular QMD consist of Ni pillars [12].

Types of nanoimprint lithography

The NIL process rapidly developed in the past decade due to its merits and potential for various applications. Several types of NIL processes were proposed for enhancing the capability and application of NIL process. The general NIL process (also named as thermal NIL or hot embossing lithography [15]) is to use a nanopatterned mold to pressed into a polymeric material (so-called resist) for nanostructured formation. During the imprinting process, both the mold and polymeric material are first heated to a temperature which is higher than the glass transition temperature of used polymeric material. Then the mold is pressed against the polymeric material coated substrate at a specific pressure and held until the temperature dropped below the glass transition temperature of polymeric material. Finally, the mold is detached from the pressed substrate (Fig. 1. 1. 1). The applied temperature and pressure need to optimize dependent on the type of polymeric material. The sub-10 nm nanopatterns with ultrahigh resolution can be fabricated by thermal NIL process has been demonstrated [3]. In addition, the metallic mold also can be applied in thermal NIL process to extend the application of thermal NIL process. However, the thermal cycling process decreases the efficiency and causes thermal mismatch between the mold and the substrate, resulting in pattern distortions or stress build-up [16] which reduces the accuracy of thermal NIL process.
The room temperature NIL process (RT-NIL) [17] is used to form nanostructures if high temperatures have to be avoided. The general principle of RT-NIL is similar with thermal NIL but without heating and cooling processes. The hydrogen silsequioxane (HSQ) [18-19] is commonly used as the resist material for RT-NIL. Because of the absence of thermal cycling process, the unwanted effects caused by heating or cooling can be ignored and the experimental processes are simplified. Nevertheless, the high applied pressure is needed in RT-NIL process, because of the high modulus of HSQ.
In ultraviolet-based NIL process (UV-NIL) [20-21], a UV-transparent mold (e.g. quartz) is pressed into an UV curable resist and held until the UV curable resist solidified through UV exposure. The UV-transparent mold is then detached from the substrate (Fig. 1. 1. 7). The UV-NIL process is performed at room temperature with low applied pressure, making it very attractive for various applications. In addition, the high alignment can be achieved due to the use of transparent mold [22].

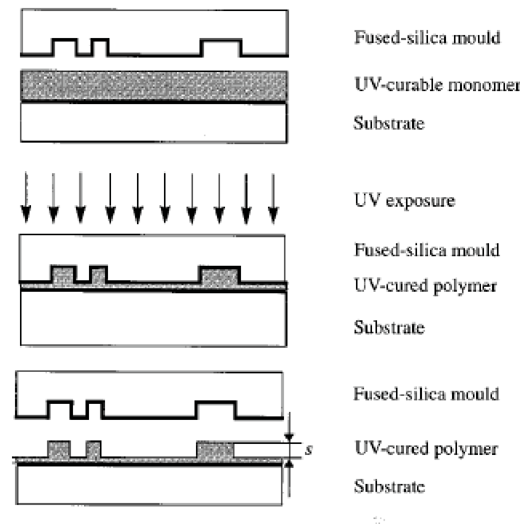

Fig. 1. 1. 7. Schematic illustrations of UV-NIL process [20].

Fabrication of imprinting mold

Because of the NIL process is based on the application of an imprinting mold to mechanically deform the polymeric materials for nanostructured fabrication. Therefore, the imprinting mold plays an important role in NIL process and is required to possess: (1) a precisely designed 3D nanostructured surface, and (2) sufficient mechanical property (e.g. hardness) during the imprint processes. The combination of electron beam lithography (EBL) and reactive ion etching (RIE) is generally applied to fabricate the imprinting mold, and the various nanopatterns can be precisely formed. The commonly used imprinting mold fabrication processes are described in Fig. 1. 1. 8. A polymeric material layer is spin-coated on a hard substrate surface and, then the desired nanopattern geometry of the polymeric material layer is defined through EBL. RIE is then applied for patterning the substrate material through a defined polymeric material layer. Finally, a mold with nanopatterns is formed after the polymeric material has been removed with an organic solvent [23-25]. The Si, SiO_2, silicon nitride, and quartz are typical materials used for imprinting mold because of sufficient hardness and compatibility with traditional fabrication process (e.g. anisotropic RIE process)

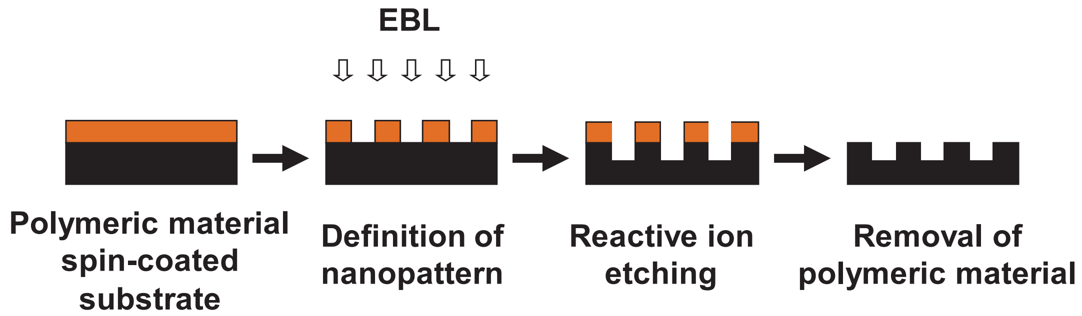

Fig. 1. 1. 8. Schematic illustrations of fabrication process of a NIL mold by EBL and RIE.

Electrochemical processes such as electrodeposition and electroless deposition are alternative candidates for imprinting mold fabrication [26-28] due to process simplicity, high throughput, and well cost performance. Metallic material (e.g., nickel alloy) as a replicate is electrodeposited on a nanopatterned SiO_2/Si master mold (coated with conductive seed layer) to copy patterns of master mold. After deposition, the master mold is removed by KOH, HF or NaOH etching (Fig. 1. 1. 9) [27-28].
On the other hand, electroless deposition (used in this thesis) is also commonly used for imprinting mold fabrication due to the merit of deposition on non-conductive substrate.

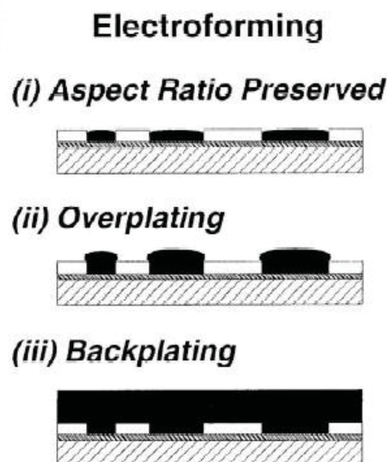

Fig. 1. 1. 9. Schematic illustrations of fabrication process of a NIL mold by electrodeposition [28].

1. 2. Electroless deposition

General principle of electroless deposition

Electroless deposition is also named as chemical or auto-catalytic deposition which occurs without the use of external electrical power. Therefore the electroless deposition is applicable to non-conductive substrates. The electroless deposition is accomplished when the metallic ion in an aqueous solution reduces on a target substrate by employing a reducing agent. The general reaction mechanism is listed as below.

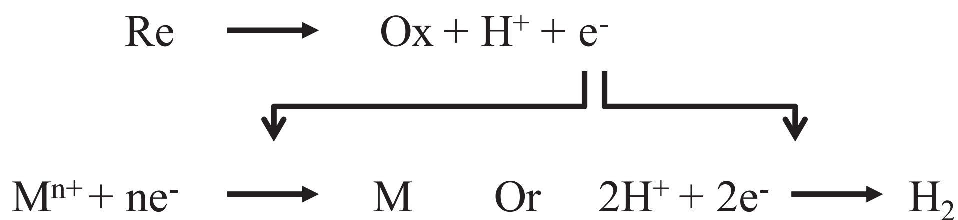

Fig. 1. 2. 1. Schematic illustrations of reaction mechanism of electroless deposition. Re: Reducing agent, M: Metal atom.

In general, the non-conductive substrate has to be catalyzed before eletroless deposition. In conventional catalyzation processes (e.g., Sn-Pd catalyzation process), the substrate has to be sensitized by Sn prior to activation of Pd, followed by the electroless deposition carried out on the catalyzed surface. Electroless deposition is widely applied with several advantages, such as;

The electroless deposition can carry out on the non-conductive substrate (such as; plastic) by catalyzation pretreatment.

The material can be deposited on the substrate with uniform thickness, even though the substrate with complex 3D structure, due to electroless deposition occurs without the use of external electrical power and the problem of non-uniform current distribution can be avoided.

The properties of deposited metallic alloy are controllable by adjusting the composition and condition of deposition bath.

Electroless NiP deposition

Since electroless Ni alloy deposition proposed by Brenner and Riddell in 1946 [29], it have been widely used in the machinery, automobile, aerospace, chemical engineering, and electronic industries, because of the deposited Ni alloy with uniform thickness, good corrosion, wear and abrasion resistance [30-35]. Electroless Ni alloy deposition bath containing reducing agent of sodium hypophosphite is commonly applied [36] because of its low cost, ease of process control, and so on. The general reaction mechanism of hypophosphite reduced electroless NiP deposition is listed in Fig. 1. 2. 2.

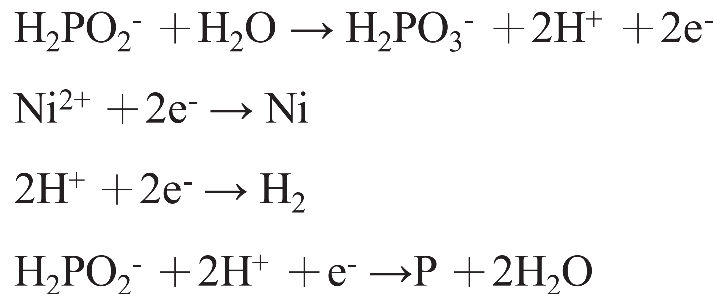

Fig. 1. 2. 2. Schematic illustrations of reaction mechanism of hypophosphite reduced electroless NiP deposition.

Merits of electroless NiP deposition

The properties of electroless NiP are easily controlled by adjusting the compositions and conditions of deposition bath. In addition, specific properties can be achieved through composite deposition and anneal treatment.

Property control of NiP

By adjusting the pH of deposition bath, the P ratio of deposited NiP can be controlled. In general, the P ratio of deposited NiP increasing with decreasing the pH of deposition bath, moreover the deposited NiP is amorphous in high P ratio (> 8 wt%), and is crystalline in low P ratio (< 7 wt%) [37]. The hardness, internal stress, and elastic modulus of deposited NiP are all controllable and dependent on the pH of deposition bath.

The SiC or PTFE nanoparticles are commonly used as additives and added into the NiP deposition bath for composite deposition. The deposited NiP-SiC with higher hardness [38] and deposited NiP-PTFE with lower friction coefficient are demonstrated [39-40]. On the other hand, the crystal property of deposited NiP can be controlled by anneal treatment. The amorphous NiP is crystallized and show better hardness performance after anneal treatment is demonstrated [41-42]. Adjusting the compositions or temperature of deposition bath also affects the properties of deposited NiP. The electrolessly deposited NiP with desired mechanical properties can be formed which is useful to fabricate an imprinting mold with desired property; therefore the electroless NiP deposition is considered one of the suitable processes for imprinting mold fabrication and used in this thesis.

1. 3. Self assembled monolayer

General principle of self assembled monolayer

Self assembled monolayer (SAM) is an ordered molecular assembly formed spontaneously and adsorbed on a substrate through a covalent bond. SAM consists of headgroup (or ligand), backbone (or chain), and endgroup (or terminal functional group) (Fig. 1. 3. 1) [43]. The head group, such as thiol, or silane is generally used to define the SAM system. For example, SAM of thiol on metal (e.g., Au) [44] and silane on oxidized surface (e.g., SiO_2) [45] are the typical systems of SAM. Backbone provides the information of SAM thickness, and also acts as a barrier [46], adhesion promoter [47], or interface lubricant [49]. The tribological properties of a surface modified by SAM of different chain length had been investigated, demonstrating that tribological lifetime is enhanced by increasing the chain length of the SAM. Endgroups (e.g., –CH3, –COOH, –NH2) determines the surface properties of SAM modified surface. The endgroups of SAM immersed in a specific solution can directly react with the molecules exist in the solution. DNA, proteins, or catalysts can be immobilized on the SAM modified surface are demonstrated [47-48, 50-57]. Furthermore, the endgroups are controllable by lithographic exposure tools to satisfy the desired purposed [58-60].

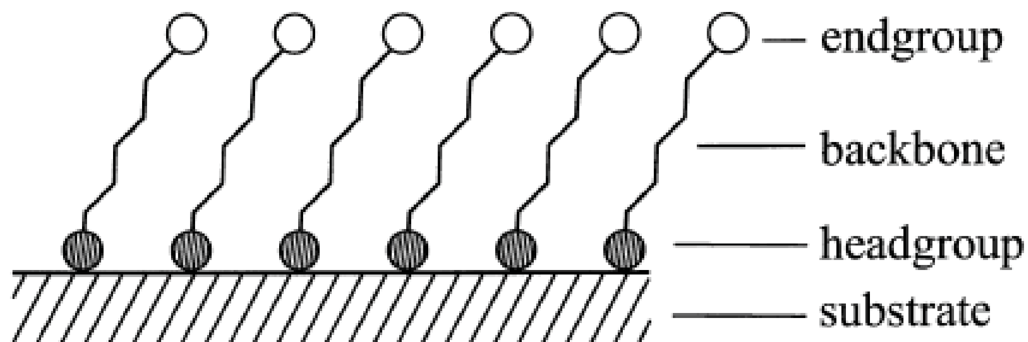

Fig. 1. 3. 1. Schematic illustrations of SAM [43].

Formation of self assembled monolayer of organosilane

Organosilane such as alkylalkoxysilane, and alkylaminosilane require hydroxylated surface for organosilane SAM formation through silane coupling reaction [47-48]. The general mechanism of silane coupling reaction is shown in Fig. 1. 3. 2. At first, alkoxy groups of organosilane are hydrolyzed. The chemisorbed crosslinked siloxane network is formed through the condensation of adjacent adsorbed silantriols with each other, and hydrogen bonds with hydroxyl groups on the substrate. At the last step, during drying or curing, the H_2O is liberated and a covalent bond is formed with the substrate [61].

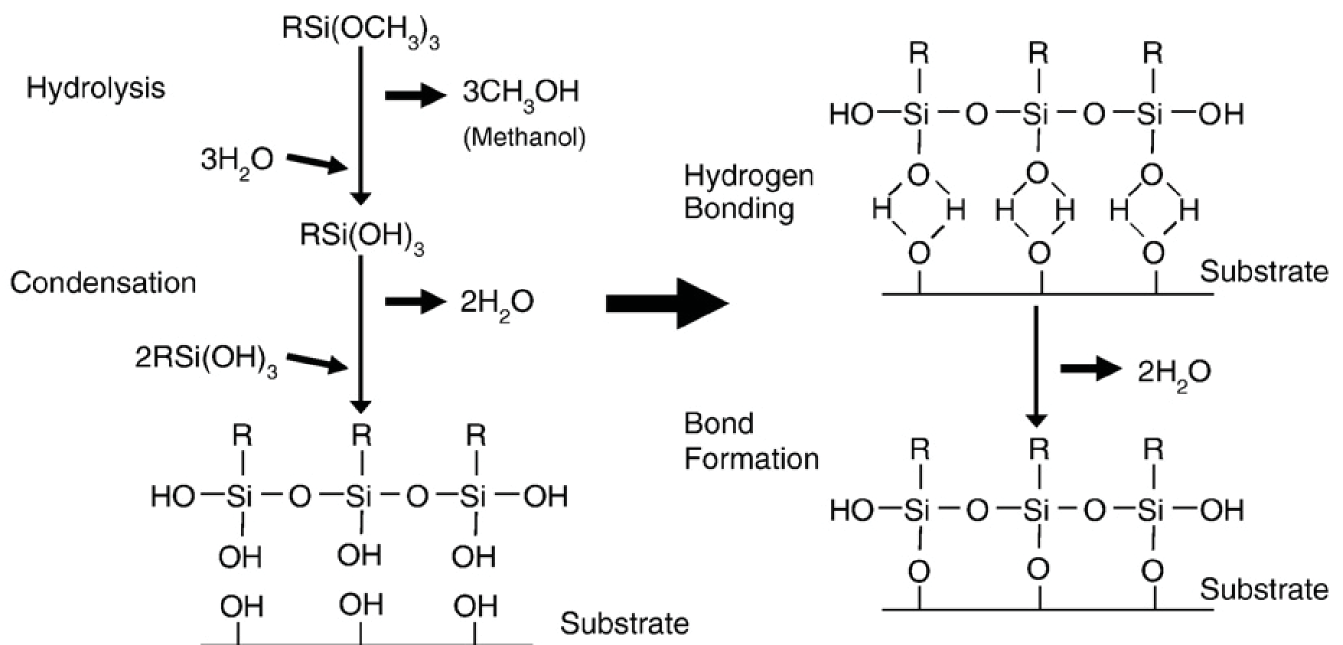

Fig. 1. 3. 2. Schematic illustrations of SAM formation process [60].

Merits of self assembled monolayer

Because SAM is a spontaneously assembled nanomaterial with ordered nanostructures and is easy to be prepared and designed, SAM is considered important and useful to modify the surface and control the properties of interfaces, such as, surface energy, corrosion, adhesion, tribology, which are strongly influenced by conditions of nanoscale surface. Moreover, SAM is widely applied in micro- and nanotechnology due to its feasibility in ultra small scale ($<$ few nm).

Applications of self assembled monolayer

SAM for pattern fabrication

SAMs are the common materials used in microcontact printing (μCP) technique for formation of patterned SAMs. In a typical experimental procedure of μCP, SAMs as ink are formed on a polydimethylsiloxane (PDMS) mold, the SAM-inked PDMS mold is pressed to the target sample for patterned SAMs transfer (Fig. 1. 3. 3). The patterned SAMs on the surface of target sample can be used to immobilize DNA, proteins, antibodies and so on. In addition, the patterned SAMs on the surface of target sample can be also used as resists for pattern fabrication on the surface of other materials.

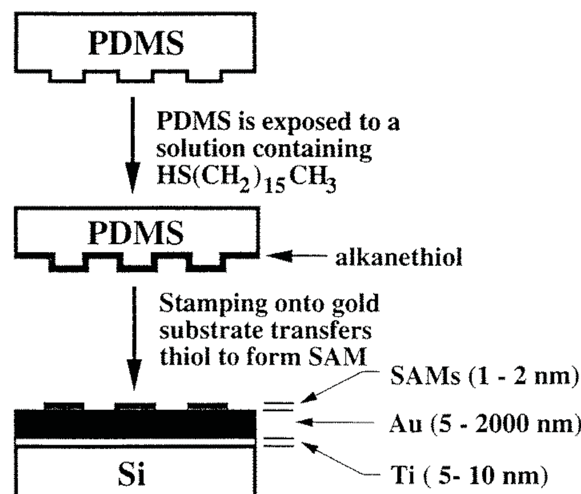

Fig. 1. 3. 3. Schematic illustrations of μCP [62].

SAM as adhesive layers

Chen et al. [63] used μCP technique to form patterned SAMs on Au surface as adhesive layers of fibronectin, and the bovine capillary endothelial (BCE) cells were cultured on such fibronectin. The cell spreading and shape could be precisely controlled by adjusting the size and interval distance of patterned SAMs (Fig. 1. 3. 4). These results provided an essential tool for investigation of cell growth and apoptosis, moreover, the possibility to control cell function.

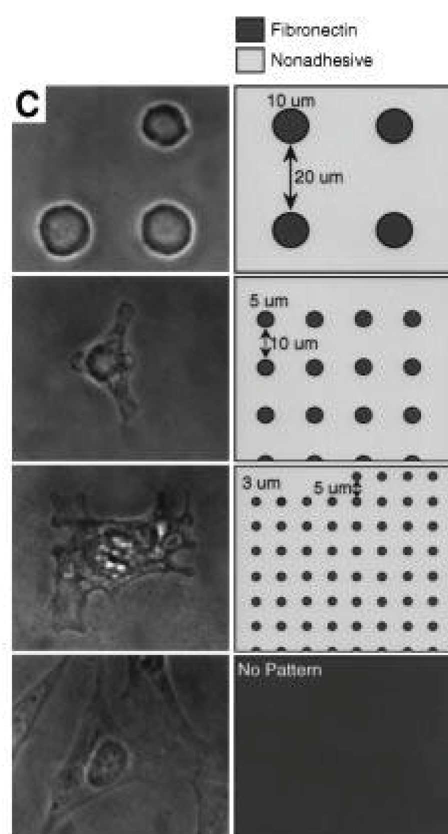

Fig. 1. 3. 4. Phase-contrast micrographs of BCE cells cultured on a substrate containing fibronectin-coated SAM circles [63].

SAM as resists

Geissler et al. [64] printed incomplete monolayers of eicosanethiol (ECT) as resist on Au to protect it from corrosion for pattern fabrication, and used octanol to heal the defects of ECT to improve the capability of corrosion resistance. In Fig. 1. 3. 5a, Au dissolved entirely in the etch bath due the imperfect ECT resist. In contrary, the ECT printed area (patterns) was remained when the etch bath contained octanol,

because of the defects of ECT were healed by octanol (Fig. 1. 3. 5b). Higher concentration of ECT made the denser monolayer formed, which protects the Au in the printed area (Fig. 1. 3. 5c) even though the etch bath without octanol. To compare with Fig. 1. 3. 5c, Au patterns with high contrast and accuracy could be remained when the etch bath contained octanol (Fig. 1. 3. 5d).

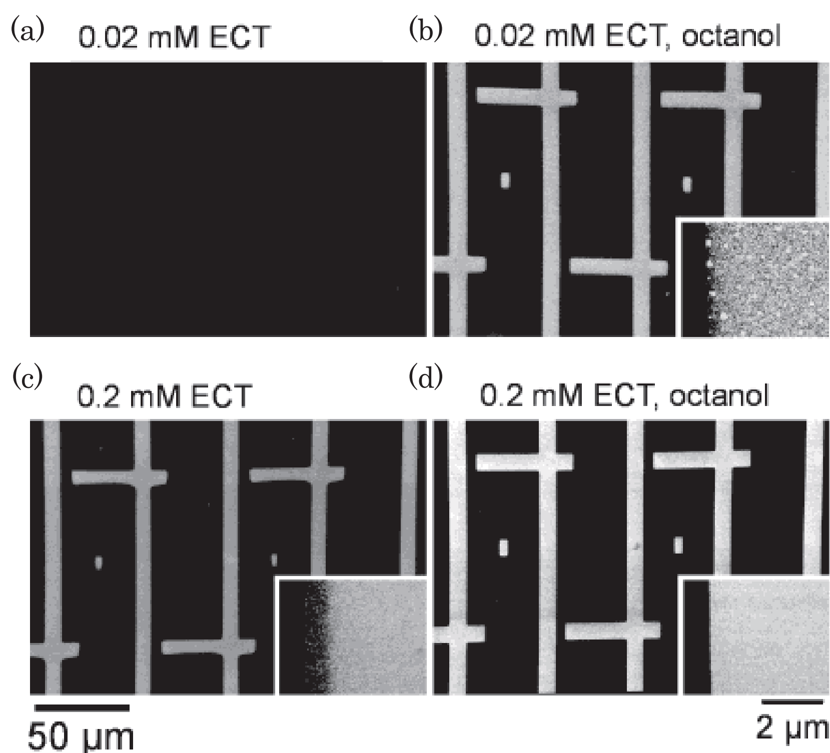

Fig. 1. 3. 5. Etch selectivity of substrates covered with ECT resists [64].

Formation of self assembled monolayer of organosilane on hydroxyl group-free surface

As mentioned before, the hydroxylated surface is necessary for organosilane SAM formation through silane coupling reaction. On the other hand, the materials, such as cyclo olefin polymer (COP), polyimide (PI), methyl silsesquioxane (MSQ), whose surface is hydroxyl group-free, require surface modification to generate hydroxyl group [65] on their surface for silane SAM formation. UV irradiation and plasma treatment are commonly used for producing hydroxyl groups.

Combination of electroless deposition and self assembled monolayer

The well stability of SAM in aqueous makes it is feasible to apply in electrochemistry, such as electroless deposition. In electroless deposition, the SAM is generally used to immobilize the Pd catalysts by coordinated reaction. There are several factors affects the conditions of Pd catalysts on the SAM. Calvert et al. [66] demonstrated that the Pd catalyst coverage on the SAM modified surface increases with increasing the treatment time, and found that catalyst coverage of 20 % was sufficient for electroless deposition. In addition, the deposited Ni alloy is affected by the Pd catalyst coverage on the SAM modified surface. The surface roughness of Ni decreases with increasing the Pd catalyst coverage.

Application

The process that combines electroless deposition and SAM receives a lot of attentions, especially in the application of integrated circuit (IC) industry [47]. The deposited metallic film on a SAM modified surface with lower surface roughness was demonstrated. In addition, the ultrathin metallic film ($<$ 30 nm) can be uniformly deposited on the SAM modified nanostructures [47-48]. In certain case, the SAM acts as adhesive layer to avoid the deposited metallic film pilling off the substrate. Osaka et al. used NiB as a diffusion barrier layer for ultra large scale integration (ULSI) interconnects. NiB with thickness of 30 nm was deposited on the trench-patterned substrate modified by Pd activated SAM (Fig. 1. 3. 6), and demonstrated that the deposited NiB with sufficient thermal stability, adhesion strength and an acceptable barrier property.

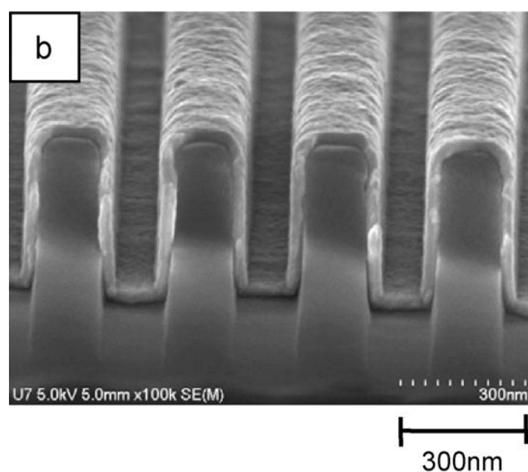

Fig. 1. 3. 6. SEM images of NiB barrier layer deposited on the SiO_2/Si

trench-patterned substrate [47].

1. 4. Nanoindentation

Because of the rapidly development in nanotechnologys, such as the components in electronic devices, ULSI, microelectromechanical systems (MEMS) are ever shrunk down from micrometer lengths to nanometer lengths in order to achieve superior functionality. Therefore materials used for these devices are also miniaturized to nanometer lengths. The accurate mechanical property measurement of such nanomaterials is strongly demanded for confirming their reliability. The indentation technique is expected to be the method for satisfying the demands and wildly developed since 1970s [67-70].

General principle of nanoindentaion

The general principle of nanoindentation is briefly described as follows: (1) a hard tip (made of diamond, diameter: 100 nm ～ few micrometer) is pressed on a sample to form an indent, (2) the mechanical properties (e.g., hardness, Young's modulus etc.) of sample can be evaluated by observing the change of applied force (so-called load-displacement curve) or the contact area of residual indent. Oliver-Pharr [71] and AFM nanoindentation [72] are the commonly used methods.

Merits of nanoindentaion

What makes nanoindentation an attractive and widely applied technique is that its facility in nanometer lengths. The mechanical properties of nanoscale materials can be precisely investigated by nanoindentation with advantages of high accuracy, low applied force, well repeatability, and so on [73-78].

Applications of merits of nanoindentaion

High accuracy in 3D nanostructure
Because of the merits mentioned above, nanoindentation is extensively applied for various purposes. Li et al. [79] used nanoindentation to investigate the hardness and elastic modulus of a silver nanowire, and the indents were successfully formed on a wire which is approximately 4 μm in long and 42 nm in diameter. The silver nanowire possesses comparable hardness and elastic modulus to those of the bulk silver was demonstrated. Furthermore, the silver nanowire could be cut in half by using a high

applied force at the desired position, indicating that the nanowire can be processed as normally done on the macroscale. Therefore, nanoindentation is also expected to be applied in nanofabrication.

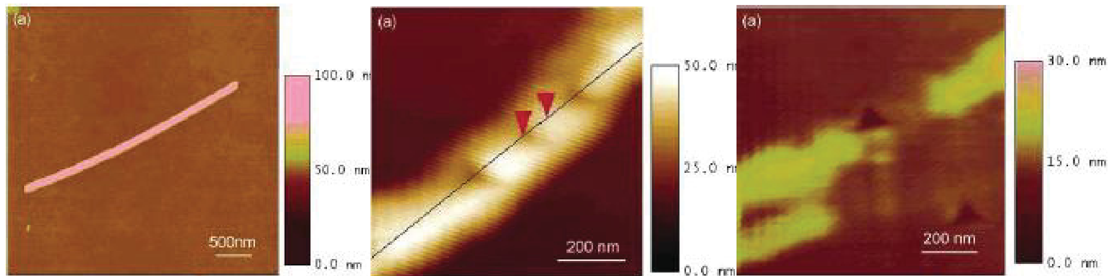

Fig. 1. 4. 1. Nanoindentation performed on a silver nanowire [79].

High accuracy in flat surface

Yang et al. [80] took advantage of high accuracy of nanoindentation and precisely performed it on an individual Ni grain of variety size for investigating the interaction between dislocations and grain boundaries in single grain. Demonstrating that in certain grain size (< 900 nm) and indentation depth, the grain boundaries act as barriers limit the movement of dislocations to affect the hardness of electrodeposited Ni.

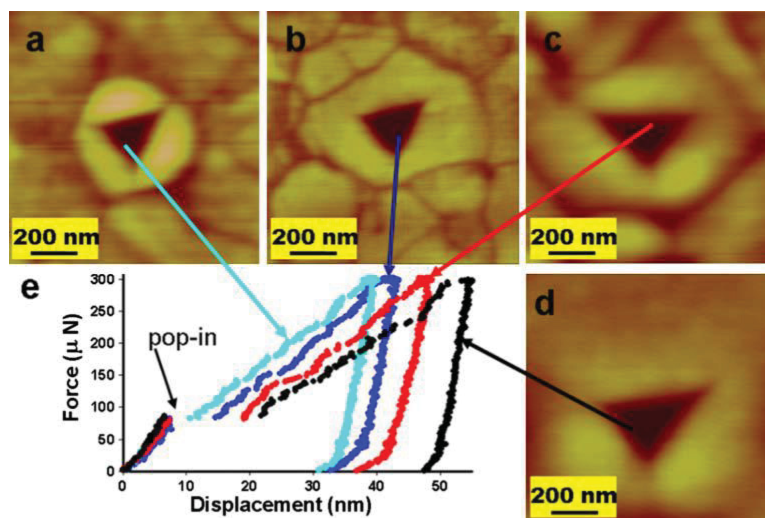

Fig. 1. 4. 2. Nanoindentation performed on variety size Ni grain [80].

Low applied force

Several indentation techniques are available to investigate the mechanical property of thin film. In order to achieve accurate investigation of mechanical property of thin films, the investigated film thickness should be five times higher than the indentation depth for avoiding the effects which come from substrate. In the case of nanoscale thin film, the accurate measurement is difficult to achieve by using conventional indentation technique, because of the substrate effects frequently generated by high applied force (mN ～ N) which causes deep indentation depth. On the other hand, the nanoindentation is alternative candidate for achieving high accurate investigation due to the use of low applied force (μN). Bhushan et al [81]. successfully carried out the nanoindentation on Si (111) surface to form ultra shallow depth (1 ～ 7 nm) and demonstrated the capability of measurement in ultra thin film.

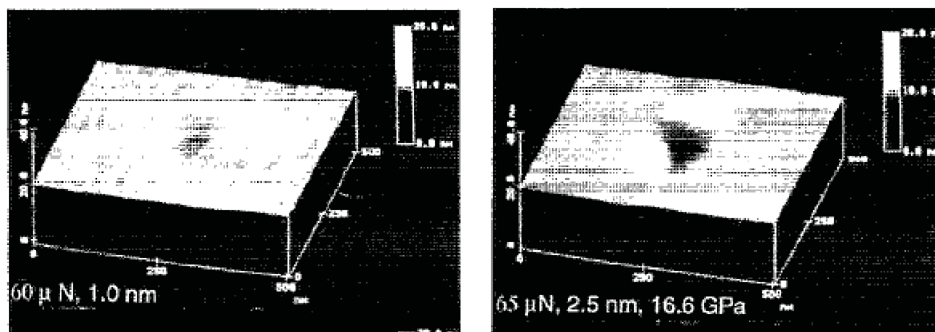

Fig. 1. 4. 3. Nanoindentation performed on Si (111) surface with ultra shallow depth [81].

1. 5. Nanoindentation analysis for hardness

Because of nanoindentaion with the property of nanoscale accuracy, it is extensively applied to investigate the hardness of 3D nanostructured material, such as nanopillar, nanowire, nanocube, and so on. Furthermore, the use of low applied force makes it is feasible to investigate the hardness of ultrathin film without substrate effects. Hardness is a property of how resistant solid matter is to permanent deformation when an external force is applied on it, and is generally described as equation (1). In general, the applied force is known and controlled by the operator. On the other hand, the contact area has to be investigated. Therefore, the accurate measurement of the contact area is essentially important to precisely estimate the hardness.

$$H = \frac{P}{A_c} \quad (1)$$

H : Hardness
P : Applied force
A_c : Contact area

In general nanoindentation process, a three sided pyramid diamond tip (Fig. 1. 5. 1a), which diameter is few hundred nanometers or few micrometers, is used. The tip with known applied force is pressed on the target sample to form the triangular indent (Fig. 1. 5. 1b). Directly observing the indent by using microscope (e.g., SEM), the contact area of residual indent can be obtained. Once we know the applied force and contact area of indent, the hardness of target sample can be easily evaluated by using equation (1).

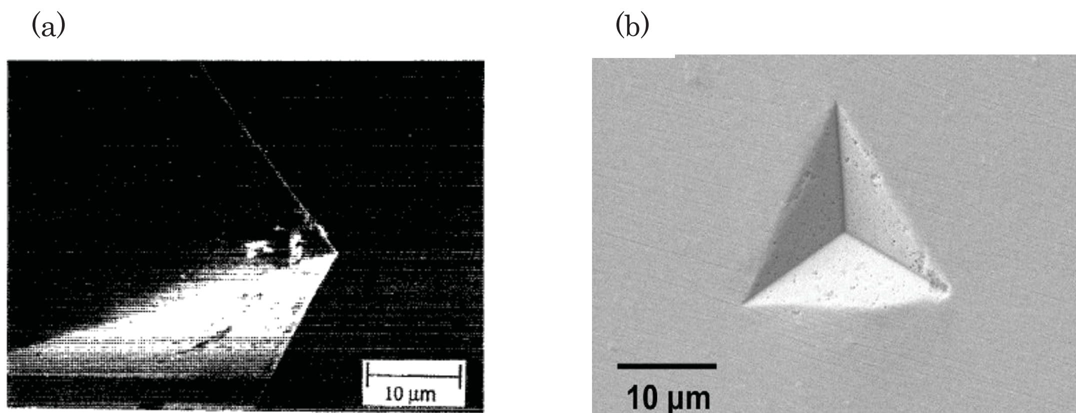

Fig. 1. 5. 1. SEM image of (a) three sided pyramid diamond tip [81], and (b) residual indent [82].

However, using SEM to observe the contact area of residual indent is time consuming and enhance the complexity of experimental processes. Therefore, several alternative approaches were proposed for easier estimation of contact area, and those approaches are briefly described as follows.

Oliver-Pharr method

The characteristic of Oliver-Pharr method is that it uses the load-displacement curve (Fig. 1. 5. 2) to estimate the "projected" area (A_p) of residual indent rather than the contact area of residual indent. The equation (1) is redefined as equation (2) in Oliver-Pharr method.

$$H = \frac{P_{max}}{A_p} \quad (2)$$

H : Hardness
P_{max} : Peak indentation load
A_p : Projected area

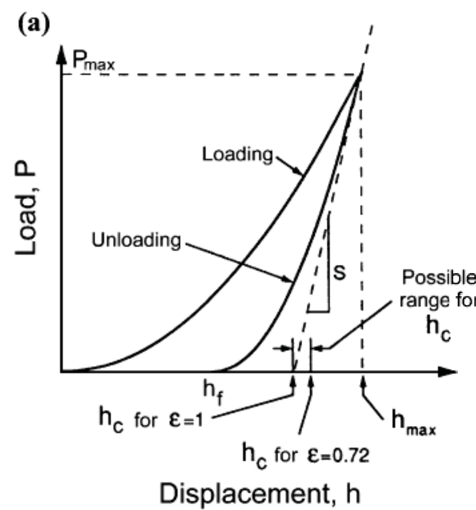

Fig. 1. 5. 2. Schematic illustrations of load-displacement curve [83].

In the case of the tip with a known geometry, the projected area is a function of the contact depth (h_c). The projected area for a perfect three sided pyramid diamond tip (Berkovich tip) is given by equation (3).

$$A_p = 24.56\, h_c^2 \quad (3)$$

The contact depth can be estimated from the load–displacement curve by using equation (4) where ε is a constant that is 0.75 for a Berkovich tip. $S = dP / dh$ is the experimentally measured stiffness which observed form the slope of the initial portion of the unloading curve. h_{max} is the depth at peak indentation load.

$$h_c = h_{max} - \varepsilon \frac{P_{max}}{S} \quad (4)$$

However, the tips used in practical nanoindentation measurement are not ideally sharp. Therefore, the calibration of equation (3) is needed for more accurate investigation. Furthermore, to compare with the true contact area, the projected area estimated by Oliver-Pharr method is frequently underestimated which results in the evaluated hardness trend to higher than the real hardness of investigated sample.

AFM nanoindentation

The high resolution of atomic force microscopy (AFM) makes it can be used to observe the surface structure at the nanometer lengths level, and the applied force can be controlled in the range of nN to pN. These properties make AFM to be an attractive alternate for nanoindetation tester. To compare with conventional nanoindentation techniques, AFM nanoindentation is more suitable for ultra tihn film measurement due to lower applied force. In addition, the contact area of residual indent can be directly observed by using AFM. AFM nanoindentation has a high suitability for the investigation of nanostructured materials has been demonstrated by many researchers. The general probe used in AFM nanoindentation is composed of rectangular stainless steel cantilever and three sided pyramid diamond tip (Fig. 1. 5. 3). The length, width and thickness of cantilever are is micrometer lengths, and the cantilever is flexible with certain spring constant (100 ～ 500 N/m). The diamond tip with few hundred nanometers in diameter is used

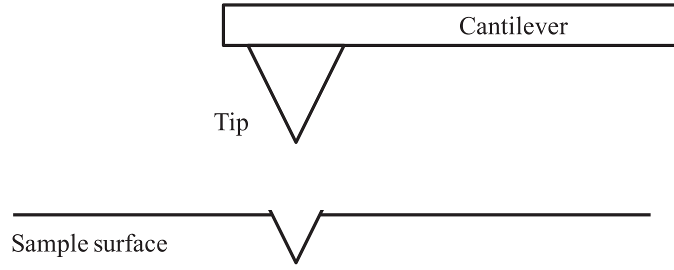

Fig. 1. 5. 3. Schematic illustrations of AFM nanoindentation.

In AFM nanoindentation, the indent is directly observed by general AFM measurement for estimating the contact area of residual indent. A typical triangular indent is observed just after the nanoindentation asvshown in Fig. 1. 5. 4. The width (l) of triangular indent can be evaluated from cross sectional image of indent. For three sided pyramid diamond tip with an apical angle of α, contact area (A_c) of residual indent is given by equation (5). The evaluated A_c is then converted in to A_p (A_p / A_c = Sinα) and substituting into equation (2) for hardness calculation. In this thesis, the AFM nanoindentation was used to investigating the hardness of NiP nanopatterns due to it could be precisely performed on the desired position for achieving accuracy measurement.

$$A_c = \frac{l^2}{\sqrt{3}\ \sin\alpha} \qquad (5)$$

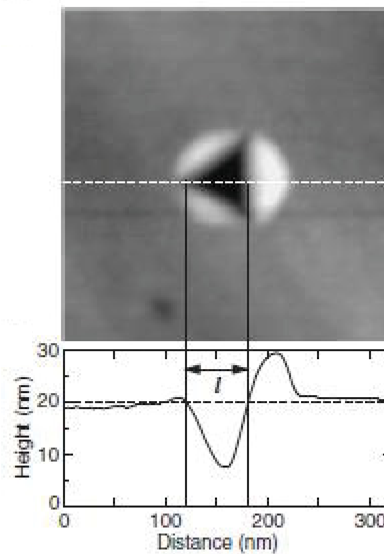

Fig. 1. 5. 4. AFM image of residual indent and its sectional image [72]

1. 6. Purpose of this thesis

NIL has been demonstrated as an effective nanofabrication process, which can be applied to electronic divices, optical elements, biosensors, and magnetic storage devices with numbers of advantages, such as high throughput, high resolution, low cost, and so on. An imprinting mold with (1) precisely designed nanopatterns and (2) sufficient mechanical property (e.g., hardness) is essential important and necessary in NIL process, due to its experimental principle (described before). In the view of requirements of NIL process, (1) the efficient fabrication processes of an imprinting mold with nanometer accuracy and (2) the accurate mechanical property analysis for verifying the imprinting mold (especially a single nanopattern of a mold) with sufficient mechanical property are key issues in the development of NIL process.

In this thesis, an electroless NiP imprinting mold was fabricated by a replication of a nanopatterned mastr mold. Moreover, the mechanical property of fabricated mold was investigated by nanoindentation.

In chapter 2, the initial catalyzation conditions of SAM on an inorganic master mold (SiO_2/Si) and their effects on the mechanical properties of deposited NiP had been systemically studied for the fabrication of nanometer accurate imprinting mold.

In chapter 3, organic polymeric master mold [cyclo-olefin polymer (COP)] was used to substitute the SiO_2 master mold. The process regarding formation of SAM and deposition of metallic material (NiP in this thesis) on a nanopatterned COP master mold had been investigated for further development of mold fabrication.

In chapter 4, the mechanical properties of fabricated imprinting mold were investigated. The nanoindentation was performed on a single nanopattern of fabricated imprinting mold for hardness investigation. In addition, the relation among initial deposition condition of NiP, size of nanopattern of master mold, and mechanical property of replicate mold had been confirmed.

References

[1] S. Y. Chou, P. R. Krauss, and P. J. Renstrom, *Appl. Phys. Lett.*, **67**, 3114 (1995)
[2] S. Y. Chou, P. R. Krauss, and P. J. Renstrom, *J. Vac. Sci. Technol. B*, **14**, 4129 (1996)
[3] S.Y. Chou, P. R. Krauss, W. Zhang, L. J. Guo, and L. Zhuang, *J. Vac. Sci. Technol. B*, **15**, 2897 (1997)
[4] W. Zhang, and S. Y. Chou, *Appl. Phys. Lett.*, **83**, 1632 (2003)
[5] D. S. Macintyre, Y. Chen, D. Gourlay, E. Boyd, D. Moran, X. Cao, K. Elgaid, C. R. Stanley, I. Thayne, and S. Thoms, *J. Vac. Sci. Technol. B*, **21**, 2783 (2003).
[6] X. Cheng, Y. T. Hong, J. Kanicki, and L. J. Guo, *J. Vac. Sci. Technol. B*, **20**, 2877 (2002)
[7] P. C. Kao, S. Y. Chu, T. Y. Chen, C. Y. Zhan, F. C. Hong, C. Y. Chang, L. C. Hsu, W. C. Liao, and M. H. Hon, *IEEE Trans. Electron Devices*, **52**, 1722 (2005)
[8] J. Wang, and H. Kostal, *Laser Focus World*, **41**, 76 (2005)
[9] D. Falconnet, D. Pasqui, S. Park, R. Eckert, H. Schift, J. Gobrecht, R. Barbucci, and M. Textor, *Nano Lett.*, **4**, 1909 (2004)
[10] W. Hu, E. K. F. Yim, R. M. Reano, K. W. Leong, and S. W. Pang, *J. Vac. Sci. Technol. B*, **23**, 2984 (2005)
[11] S. Y. Chou, *Proc. IEEE*, **85**, 652 (1997)
[12] W. Wu, B. Cui, X. Y. Sun, W. Zhang, L. Zhuang, L. S. Kong, S. Y. Chou, *J. Vac. Sci. Technol. B*, **16**, 3825 (1998)
[13] T. Glinsner, P. Hangweier, H. Luesebrink, P. Dorsey, A. Homola, and D. Wachenschwanz, *Solid State Technol.*, **48**, 51 (2005)
[14] G. M. McClelland, M. W. Hart, C. T. Rettner, M. E. Best, K. R. Carter, and B. D. Terris, *Appl. Phys. Lett.*, **81**, 1483 (2002)
[15] H. Schift, R. W. Jaszewski, C. David, and J. Gobrecht, *Microelectron. Eng*., **46**, 121 (1999).
[16] Hirai Y, Fujiwara M, Okuno T, Tanaka Y, Endo M, Irie S, Nakagawa K and Sasago M *J. Vac. Sci. Technol.*, **B19**, 2811 (2001)
[17] 223 D.-Y. Khang, H. Yoon, and H. H. Lee, Adv. Mater. (Weinheim, Ger.) **13**, 749 (2001).
[18] Y. Igaku, S. Matsui, H. Ishigaki, J. Fujita, M. Ishida, Y. Ochiai, H. Namatsu, M. Komuro, and H. Hiroshima, *Jpn. J. Appl. Phys. Part 1*, **41**, 4198 (2002)
[19] S. Matsui, Y. Igaku, H. Ishigaki, J. Fujita, M. Ishida, Y. Ochiai, H. Namatsu, and M. Komuro, *J. Vac. Sci. Technol. B*, **21**, 688 (2003)
[20] J. Haisma, M. Verheijen, K. van den Heuvel, and J. van den Berg, *J. Vac. Sci.*

Technol. B, **14**, 4124 (1996)
[21] B. Vratzov, A. Fuchs, M. Lemme, W. Henschel, and H. Kurz, *J. Vac. Sci. Technol. B*, 21, 2760 (2003)
[22] A. Fuchs, B. Vratzov, T. Wahlbrink, Y. Georgiev, and H. Kurz, *J. Vac. Sci. Technol. B*, **22**, 3242 (2004).
[23] A. N. Broers, A. C. F. Hoole, and J.M. Ryan, *Microelectron. J.*, **32**, 131 (1996)
[24] A. N. Broers, J. M. E. Harper, and W. W. Molzen, *Appl. Phys. Lett.*, **33**, 392 (1978)
[25] M. D. Austin, H. X Ge, W. Wu, M. T Li, Z. N Yu, D. Wasserman, S. A. Lyon, and S. Y. Chou, *Appl. Phys. Lett.*, **84**, 5299 (2004)
[26 P. Palermo, A. Korpel, G. Dickinson, and W. Watson, *Opt. Laser. Technol.*, **9**, 169 (1977)
[27] Y. Hirai, S. Harada, S. ISAKA, M. Kobayashi, and Y. Tanaka, *Jpn. J. Appl. Phys.*, **41**, 4186 (2002)
[28] L.J. Heyderman, H. Schift, C. David, B. Ketterer, M. Auf der Maur, and J. Gobrecht, *Microelectron. Eng.*, **57**, 375 (2001).
[29] A. Brenner and G. E. Riddell, *Res. Natl. US Bur. Stand.*, **37**, 31 (1946)
[30] F.N. Hubbell, *Trans. IMF*, **56**, 65 (1978)
[31] F.N. Hubbell, *Plat. Surf. Finish.*, **65**(12), 58 (1978).
[32] L. Brown, *Trans. IMF*, **63**, 139 (1985)
[33] K. Parker, *Plat., 61(9)*, **834** (1974)
[34] A.J. Gould, *Trans. IMF*, **66**, 58 (1988)
[35] G. Straffelini, D. Colombo and A. Molinari, *Wear*, **236**, 179 (1999)
[36] R. C. Agarwala, and V. Agarwala, *S¯adhan¯a,* **28**, 475 (2003)
[37] J. Y. Song, and Jin Yu, *Thin Solid Films*, **415**, 167 (2002)
[38] Y. Li, *Plat. Surf. Finish.*, **84**(11), 77 (1997)
[39] S. S. Tulsi, *Finish.*, **7**(11), 14 (1983)
[40] S. S. Tulsi, *Trans. IMF*, **61**, 147 (1983)
[41] Y. Xiang, J. Zhang, and C. Jin, *Plat. Surf. Finish.*, **88**(2), 64 (2001)
[42] J.K Dennis, S.T. Sheikh and E.C. Silverstone, *Trans. IMF*. **59**, 118 (1981)
[43] F. Schreiber, *Prog. Surf. Sci.*, 65, 151 (2000)
[44] R.G. Nuzzo, and D.L. Allara, *J. Am. Chem. Soc.*, **105**, 4481 (1983)
[45] J. Sagiv, *J. Am. Chem. Soc.*, **102**, 92 (1980)
[46] G.J. Kluth, C. Carraro, and R. Maboudian, *Phys. Rev. B*, **59**, R10449 (1999)
[47] M. Yoshino, T. Masuda, T. Yokoshima, J. Sasano, Y. Shacham-Diamand, I. Matsuda, T. Osaka, Y. Hagiwara, and I. Sato, *J. Am. Chem. Soc.*, **154**(3),D122 (2007)
[48] M. Yoshino, H. Aramaki, I. Matsuda, Y. Okinaka and T. Osaka, *Electrochem. Solid-State Lett.*, **12**, D19 (2009)

[49] J. Ruehe, V. J. Novotny, K. K. Kanazawa, T. Clarke, and G. B. Street, *Langmuir*, **9,** 2383 (1993)
[50] K.L. Prime, and G.M. Whitesides, *Science*, 252, 1164 (1991)
[51] L. Hauûling, W. Knoll, H. Ringsdorf, F.-J. Schmitt, and J. Yang, Makromol. *Chem. Macromol. Symp.*,**46**, 145 (1991)
[52] R. Singhvi, A. Kumar, G.P. Lopez, G.N. Stephanopoulos, D.I.C. Wang, G.M. Whitesides, and D.E. Ingber, *Science*, **264**, 696 (1994)
[53] M. J. Wirth, R.W.P. Fairbank, H.O. Fatunmbi, *Science*, **275**, 44 (1997)
[54] J. Lahiri, L. Isaacs, B. Grzybowski, J.D. Carbeck, and G.M. Whitesides, *Langmuir*, **15**, 7186 (1999)
[55] N. Higashi, M. Takahashi, and M. Niwa, *Langmuir*, **16**, 1793 (2000)
[56] R. M. Nyquist, A.S. Eberhardt, L.A. Silks III, Z. Li, X. Yang, and B.I. Swanson, *Langmuir*, **16**, 1793 (1998)
[57] P. Harder, M. Grunze, R. Dahint, G.M. Whitesides, P.E. Laibinis, *J. Phys. Chem. B*, **10**, 2426 (1998)
[58] K. K. Berggren, A. Bard, J.L. Wilbur, J.D. Gillaspy, A.G. Helg, J.J. McClelland, S.L. Rolston, W.D. Phillips, M.P. Prentiss, G.M. Whitsides, *Science*, **269**, 1255 (1995)
[59] S. B. Hill, C.A. Haich, F.B. Dunning, G.K. Walters, J.J. McClelland, R.J. Celotta, H.G. Craighead, J. Han, D.M. Tanenbaum, *J. Vac. Sci. Technol. B*, **17**, 1087 (1999)
[60] P. Engels, S. Salewski, H. Levsen, K. Sengstock, and W. Ertmer, *Appl. Phys. B*, **69**, 407 (1999)
[61] G.L. Witucki, *J. Coat. Technol.*, **65**, 57 (1993)
[62] J. L. Wilbur, A. Kumar, H. A. Biebuyck, E. Kim, and G. M Whitesides, *Nanotechnology*, **7**, 452 (1996).
[63] C. S. Chen, M. Mrksich, S. Huang, G. M. Whitesides, and D. E. Ingber, *Biotechnol. Prog.*, **14**, 356 (1998)
[64] M. Geissler, H. Schmid, A. Bietsch, B. Michel, and E. Delamarche, *Langmuir*, **18**, 2374 (2002)
[65] K. S. Siow, L. Britcher, S. Kumar, H. J. Griesser, *Plasma Process. Polym.*, **3**, 392 (2006)
[66] S. L. Brandow, W. J. Dressick, C. R. K. Marrian, G. M. Chow, and J. M. Calvert, *J. Electrochem. Soc.*, **142**, 2233 (1995)
[67] F. Frohlich, P. Grau, and W. Grellmann, *Phys. Stat. Sol. (a)*, 42, 79 (1977)
[68] D. Newey, M. A. Wilkins, and H.M. Pollock, *J. Phys. E: Sci. Instrum.*, **15**, 119 (1982)
[69] J. L. Loubet, J. M. Georges, O. Marchesini, and G. Meille, *J. Tribol.*, **106**, 43 (1984)

[70] J. B. Pethica, R. Hutchings, and W. C. Oliver, *Philos. Mag. A*, **48**, 593 (1983)
[71] W. C. Oliver, and G. M. Pharr, *J. Mater. Res.*, **7**, 1564 (1992)
[72] K. Miyake, S. Fujisawa, A. Korenaga, T. Ishida, and S. Sasaki, *Jpn. J. Appl. Phys.*, **43**, 4602 (2004).
[73] M. F. Doerner, and W. D. Nix, *J. Mater. Res.*, **1**, 601 (1986)
[74] G. M. Pharr, and W. C. Oliver, *MRS Bull.*, **17**, 28 (1992)
[75] J.L. Loubet, J.M. Georges, O. Marchesini, and G. Meille, *J. Tribology*, **106**, 43 (1984)
[76] W.C. Oliver, *MRS Bull.*, **11**, 15 (1986)
[77] W.D. Nix, *Metall. Trans.*, **20A**, 2217 (1989)
[78] J.B. Pethica, R. Hutchings, and W.C. Oliver, *Philos. Mag.*, **A 48**, 593 (1983)
[79] X. Li, H. Gao, C. J. Murphy, and K. K. Caswell, *Nano Lett.*, **3**, 1495 (2003)
[80] B. Yang, and H. Vehoff, *Acta. Mater.*, **55**, 849 (2007).
[81] B. Bhushan and V. N. Koinkar, *Appl. Phys. Lett.*, **64**, 1653 (1994);
[82] M.A. Dudek, N. Chawla, *Intermetallics*, **18**, 1016 (2010)
[83] X. Li, B. Bhushan, *Mater. Charact.*, **48**, 11 (2002)

Chapter 2

Initial catalyzation analysis of SAM modified SiO_2 surface for electroless NiP imprinting mold fabrication

2. 1. Introduction

In NIL process, the hard material (e.g., SiO_2 or quartz) is commonly used as the material of imprinting mold because of its sufficient hardness and the precise nanopatterns can be formed through EBL and RIE processes [1-3]. However, the delicate property of SiO_2 makes the damage to nanopatterns of SiO_2 imprinting mold frequently occurs during the imprint process, or the SiO_2 imprinting mold break to pieces when it fall on the floor due to people's careless. The breakage of SiO_2 imprinting mold decrease the precision and reliability of NIL process, resulting in the fabrication of a new imprinting mold is required. Nevertheless, the fabrication of SiO_2 imprinting mold with high costs, such as the high price of SiO_2 wafer, EBL, and RIE equipments, the EBL and RIE processes are energy and time consuming. All the issues mentioned above decrease the cost performance and limit the development of NIL.

On the other hand, the process that uses the SiO_2 mold as a "master mold" let the metallic material (e.g., Ni alloy) deposit on its surface to copy the nanopattern geometry of master mold, the metallic material is then detached from the master mold as a "replicate mold" is one of the potential methods of imprinting mold fabrication. Because of the metallic mold can be mass-produced by reusing the SiO_2 master mold to decreases the cost of mold fabrication, making the metallic mold tend to disposable in the case of damage generation.

Electrochemical processes such as electrodeposition and electroless deposition are attractive candidates to deposit metallic material on a SiO_2 master mold for mold replication [4, 5], due to ease process, large scale producibility, and well cost performance. Nevertheless, non-uniform deposition occasionally occurs for substrate surfaces with complex 3D nanostructures, resulting in defect formation (e.g., voids) in deposited metallic material and low nanopatterned replication ability [6-9]. Furthermore, strong adhesion strength between deposit and master mold tends to break the surface nanopatterns of detached replicate mold. In the situation of weak adhesion strength, the nanopatterns of master mold cannot be fully replicated and the deposit tends to peel off from the master mold.

In this chapter, NiP as a replicate mold was electrolessly deposited on a SiO_2 master mold, whose surface was modified with 3-[2-(2-aminoethylamino)ethylamino]propyltrimethoxysilane (TAS) (Fig. 2. 1. 1) and Pd activation (TAS-Pd catalyzation process).

From section 2. 3. 1 to 2. 3. 6, comparisons between the conventional Sn-Pd and SAM-Pd (SAM: TAS within these sections) catalyzation process were done, including

the surface morphology of substrate after catalyzation process, Pd catalyst coverage, the surface morphology of deposited NiP, adhesion strength between deposited NiP and master mold, the surface morphology of replicate mold.

In section 2. 3. 9, in order to understand the effects of amino group number of SAM on the initial catalyzation conditions and mechanical properties of NiP, the 3-aminopropyltriethoxysilane (APTES) (Fig. 2. 1. 2), which possesses one amino group, was employed to compare with TAS, which possesses three amino groups.

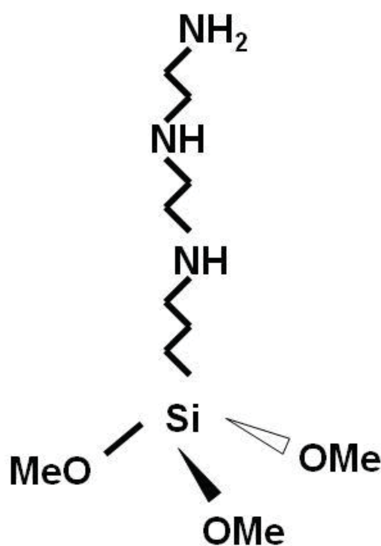

Fig. 2. 1. 1 Schematic illustration of TAS

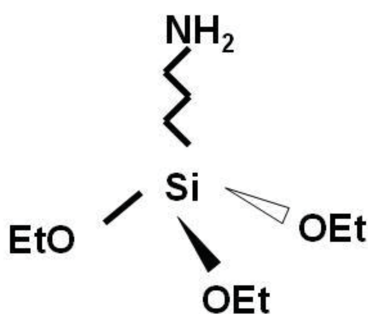

Fig. 2. 1. 2 Schematic illustration of APTES

2. 2. Experimental Methods

Substrate Clean:
The SiO_2/Si substrates were rinsed in sulfuric peroxide mixture solution (SPM, H_2O_2:H_2SO_4 = 1:3) for 10 min, followed by rinsing in deionized water (Milli-Q) before the catalyzation processes and NiP electroless deposition.

Sn-Pd Catalyzation Process:
The SiO_2 substrate was sequentially immersed into a $SnCl_2$-containing HCl solution (Table 2. 2. 1) and a $PdCl_2$-containing HCl solution (Table 2. 2. 2) for 1 min each. The above processes were repeated twice and the substrate was rinsed with deionized water between each step.

TAS-Pd Catalyzation Process:
TAS was formed on the cleaned SiO_2 substrate surface by immersing the substrate into a toluene solution mixed with TAS (97%, Aldrich Inc.) (Table 2. 2. 3) [10] for 10 min with subsequent rinsing in methanol for another 10 min and ultrasonication to remove the excess amount of silane. The TAS formed substrate was dipped into a $PdCl_2$-containing HCl solution for 30 s (Table 2. 2. 2). The substrate was subsequently treated in dimethylamineborane (DMAB: 0.05 mol L^{-1}) solution for 1 min to ensure the Pd ions were reduced to Pd metallic particles, and rinsed in deionized water between each step.

APTES-Pd Catalyzation Process:
APTES was formed on the cleaned SiO_2 substrate surface by immersing the substrate into a toluene solution mixed with APTES (99%, Aldrich Inc.) (Table 2. 2. 4) [10] for 10 min with subsequent rinsing in methanol for another 10 min and ultrasonication to remove the excess amount of silane. The APTES formed substrate was dipped into a $PdCl_2$-containing HCl solution for 30 s (Table 2. 2. 2). The substrate was subsequently treated in dimethylamineborane (DMAB: 0.05 mol L^{-1}) solution for 1 min to ensure the Pd ions were reduced to Pd metallic particles, and rinsed in deionized water between each step.

The electroless deposition bath composition and experimental conditions are shown in table 2. 2. 5. NiP was electrolessly deposited on a catalyzed nanopatterned master mold [by either the Sn-Pd or SAM-Pd (SAM: TAS or APTES) catalyzation process] prior to Ni electrodeposition. The deposits (NiP and Ni) were finally detached from

the nanopatterned master mold (Fig. 2. 2. 1). A trench-patterned master mold with nanopattern whose width and height are 300 nm (Fig. 2. 2. 2) and dot-patterned master mold with nanopattern whose diameter is 200 nm (Fig. 2. 2. 3) were used.
Surface morphology was observed by field emission scanning electron microscopy (FE-SEM, HITACHI, S-4800), atomic force microscopy (AFM, BRUKER, NanoScope IIIa), and transmission electron microscopy (TEM, JEOL, JEM-2100F). Pd catalyst coverage was measured by field emission Auger electron spectroscopy (FE-AES, JEOL, JAMP-9500F). The mechanical properties of the electroless deposited NiP were investigated using a thin film mechanical property tester (NEC, MH4000). The amount of Pd catalyst was measured by glow discharge optical emission spectroscopy in glow discharge (GDOES, HORIBA, JY5000F)

Table 2. 2. 1
The compositions of sensitized solution

Chemicals	Concentration (mol L^{-1})
$SnCl_2 \cdot 2H_2O$	0.043
HCl	0.120

Table 2. 2. 2
The compositions of activation solution

Chemicals	Concentration (mol L^{-1})
$PdCl_2$	0.001
HCl	0.030

Table 2. 2. 3
The composition of TAS solution

Chemicals	Concentration
TAS	0.1 ml
Toluene	10 ml
Temperature	60℃

Table 2. 2. 4

The composition of APTES solution

Chemicals	Concentration
APTES	0.1 ml
Toluene	10 ml
Temperature	60℃

Table 2. 2. 5

Compositions of electroless deposition bath and experimental conditions

Chemicals	Concentration (mol L^{-1})
CH_3COONH_4	0.4
$NiSO_4 \cdot 6H_2O$	0.1
$NaH_2PO_2 \cdot H_2O$	0.2
pH	5.5
Temperature	55 ℃

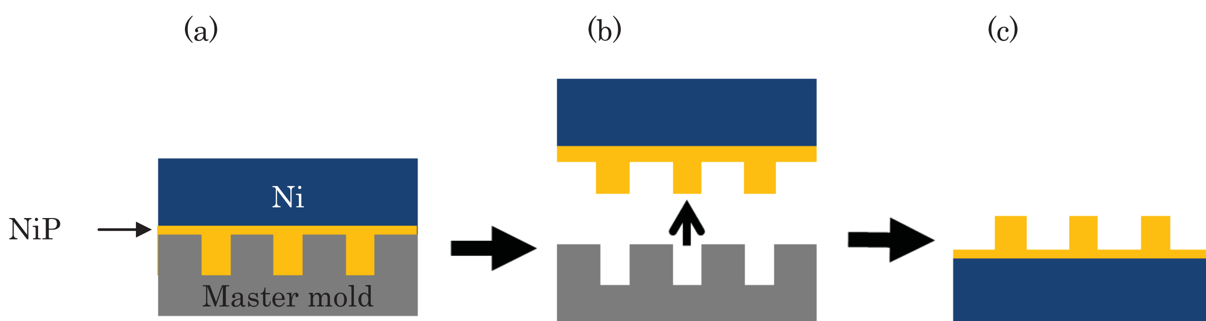

Fig. 2. 2. 1. Experimental processes: (a) NiP with controlled thickness was electrolessly deposited on SAM-Pd catalyzed master mold prior to Ni electro-deposition (b) Deposit was detached from a master mold (c) Detached NiP with nanopatterns replicated from master mold

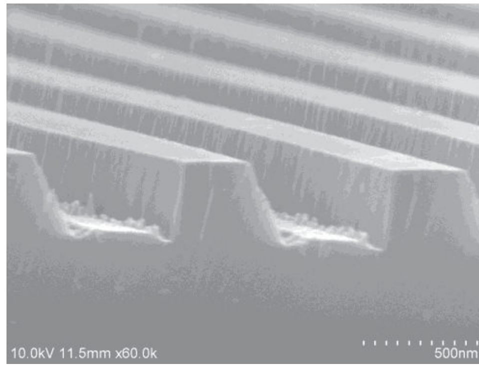

500 nm

Figure 2. 2. 2. FE-SEM images of trench-patterned master mold.

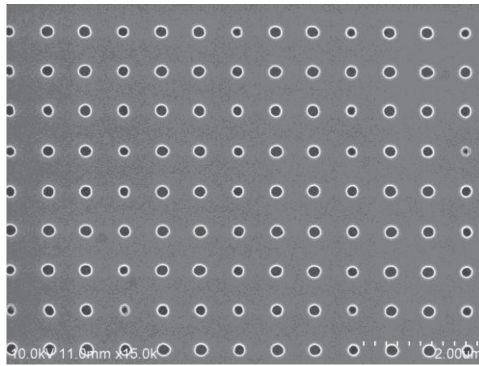

2 μm

Figure 2. 2. 3. FE-SEM images of dot-patterned master mold.

2. 3. Results and Discussion

2. 3. 1. The surface morphology of a flat SiO_2 substrate after initial catalyzation

The surface morphology on a TAS-Pd modified substrate with lower surface roughness was observed. A flat SiO_2 (without nanopatterns) substrate was used for analysis of the surface morphology of a substrate which was catalyzed by the either Sn-Pd or TAS-Pd catalyzation process. Based on the AFM results, some particles appeared after the catalyzation process, confirming the formation of Pd catalysts on the substrate (Fig. 2. 3. 1b and 2. 3. 1c). The average surface roughness (Ra) of the substrate after the TAS-Pd catalyzation process was 0.20 nm, which is much lower than that of the surface modified by the Sn-Pd catalyzation process (Ra = 1.23 nm), indicating that surface smoothness was improved by employing SAM.

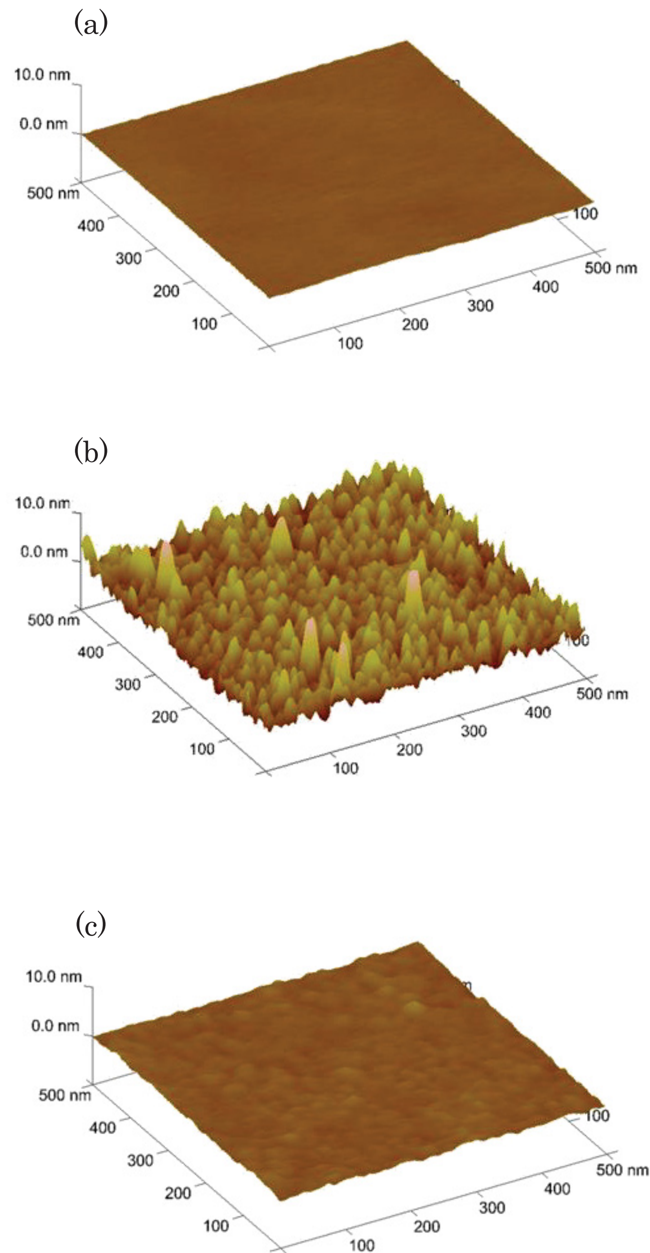

Fig. 2. 3. 1. Morphology of flat SiO_2 substrates measured by AFM: (a) before catalyzation, after (b) Sn-Pd or (c) TAS-Pd catalyzation process.

2. 3. 2. Pd catalyst coverage on a flat SiO_2 substrate after initial catalyzation

Pd catalyst coverage was better on a TAS-Pd modified surface than on a Sn-Pd modified substrate was confirmed by AES mapping. The different colors in Fig. 2. 3. 2 correspond to the different AES intensity [dN/dE, arb. units, N (E): intensity of signal from Auger electronics, and E (eV): kinetic energy of Auger electrons] of Pd element, and the intensity was directly proportional to the amount of Pd catalyst. In other words, Pd catalysts existed in colorful regions, but no Pd catalysts in dark region on a catalyzed substrate surface. In the case of low magnification of AES mapping, there were several Pd catalyst aggregates were observed on the Sn-Pd modified surface (Fig. 2. 3. 2a). In contrary, the Pd catalysts uniformly dispersed on the TAS-Pd modified surface and there were no Pd catalyst aggregates were observed (Fig. 2. 3. 2b), which was attributed to the inherent uniform formation of SAM resulting in the uniform formation of Pd catalyst.

In the case of high magnification of AES mapping, most of the TAS-Pd modified surface was covered by Pd catalysts was confirmed (Fig. 2. 3. 2d). The three amino groups in an individual TAS molecule are supposed to stably coordinate with one Pd ion, causing higher density formation of Pd catalysts on the TAS-Pd modified surface [10]. On the other hand, the dark regions on the Sn-Pd catalyzed surface represent an area with few or no Pd catalysts, thus indicating lower coverage (Fig. 2. 3. 2c). Additionally, Pd catalyst coverage is expected to increase with the duration of the Pd activation process treatment [11]. In this study, the total Pd activation (treatment) time in the Sn-Pd catalyzation process was 120 s, which is four times longer than that of the TAS-Pd catalyzation process (30 s). However, Pd catalyst coverage on the TAS-Pd catalyzed surface was apparently better. This is ascribed to the improvement from employing SAM.

Fig. 2. 3. 3. shows the representative cross-sectional TEM bright field images of catalyzed surfaces. Pd catalysts (or Pd nuclei) are smoothly and contiguously formed on the TAS-Pd catalyzed surface. However, Pd catalysts are formed on the Sn-Pd catalyzed surface with rougher morphologies and defects (indicated by red arrows). The TEM results correspond to the AFM results, with lower surface roughness on the TAS-Pd catalyzed surface. The contiguous morphology of the Pd catalyst on the TAS-Pd catalyzed surface is attributed to higher Pd catalysts coverage (Fig. 2. 3. 2d).

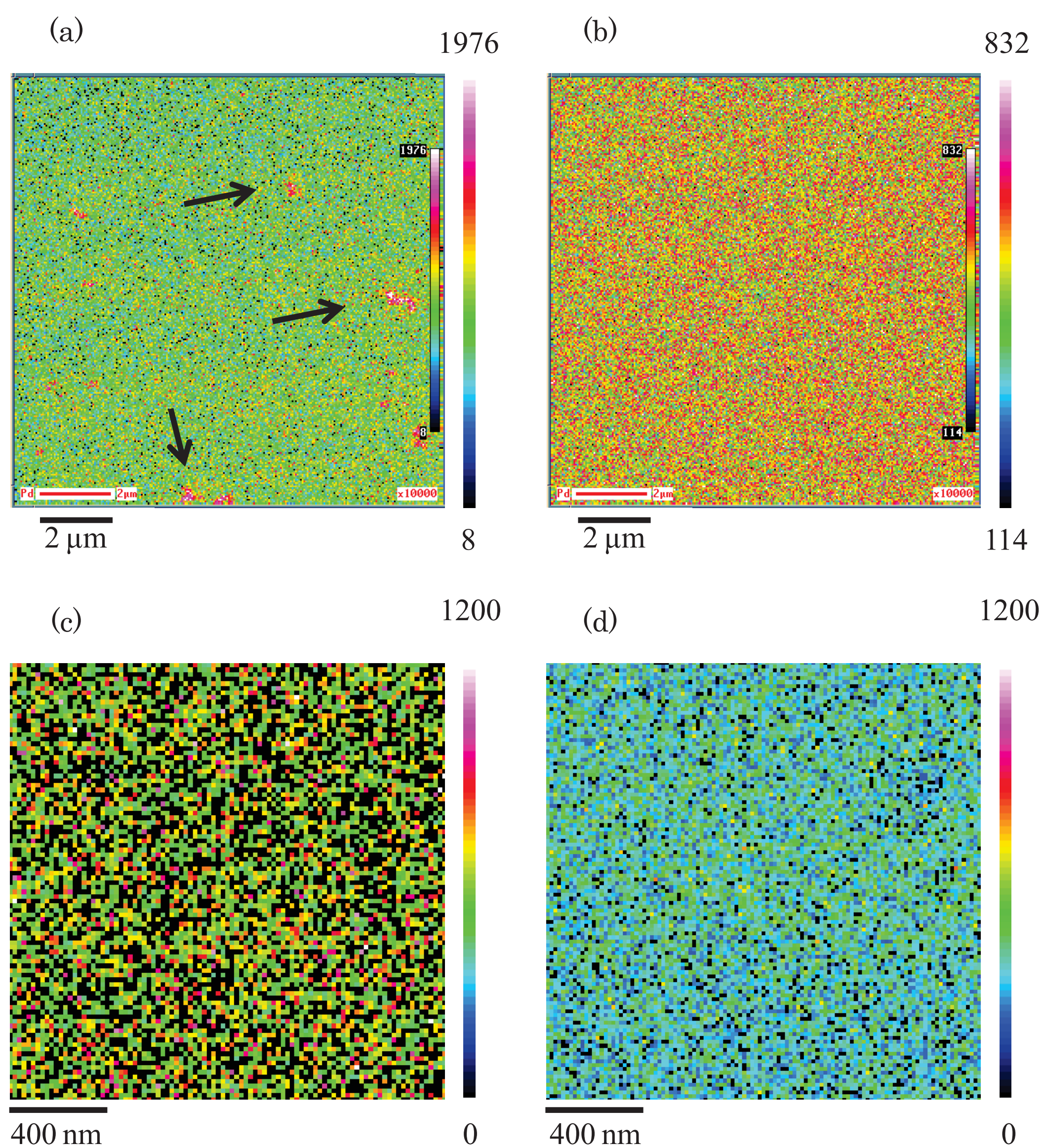

Fig. 2. 3. 2. Pd mapping data by AES of flat SiO_2 substrates after (a) (c) Sn-Pd or (b) (d) TAS-Pd catalyzation process

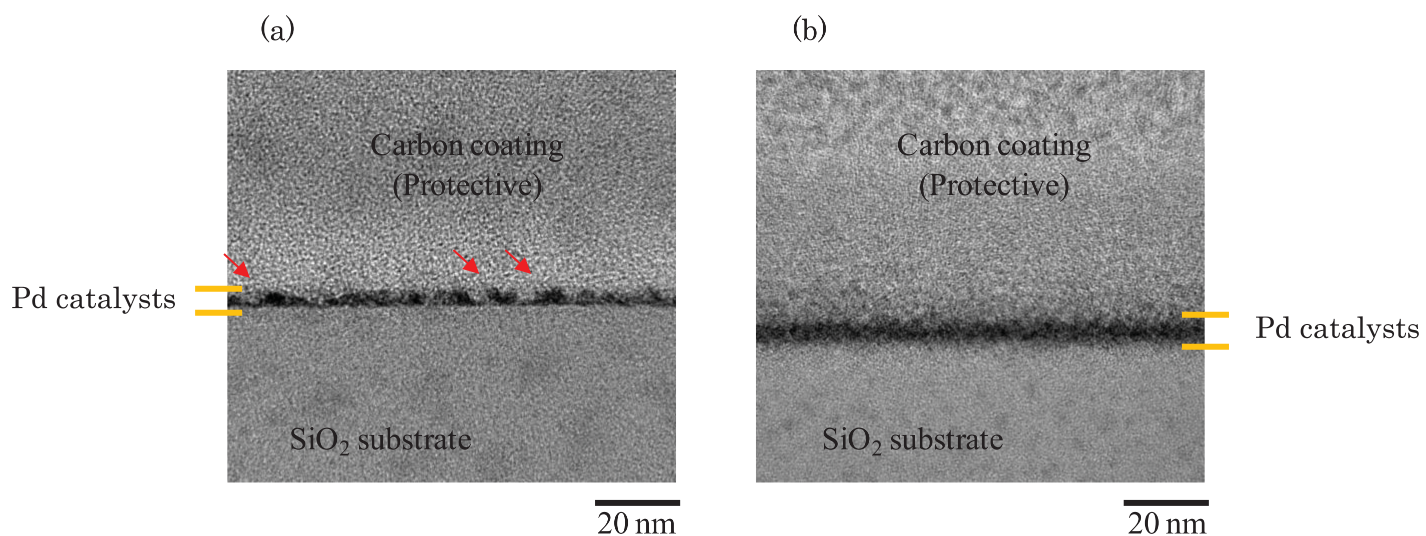

Fig. 2. 3. 3. Sectional TEM images of flat SiO_2 substrates after (a) Sn-Pd or (b) TAS-Pd catalyzation process

2. 3. 3. The surface morphology of electroless deposited NiP on a flat SiO_2 substrate

Fig. 2. 3. 4a and b shows SEM images of the initial stage (within 30 s) of the electroless NiP deposition. The TAS-Pd catalyzed surface shows distinctly greater and denser NiP particle deposition (Fig. 2. 3. 4b), which is attributed to high Pd catalyst coverage. Moreover, as deposition time increases, the electroless deposited NiP turns into a contiguous film (approximately 75 nm thick) and shows denser morphology and smaller grain size on the TAS-Pd catalyzed substrate (Fig. 2. 3. 4d). The higher the Pd catalyst coverage, the shorter the distance between Pd nuclei, reducing the spaces for NiP lateral growth and thus accelerating the vertical growth of NiP [12]. As a result, a NiP layer with denser morphology and smaller grain size is deposited on the TAS-Pd catalyzed substrate. According to previous work [11], the surface roughness of the Ni alloy was found to be linearly dependent on the coverage of Pd catalysts in which a smoother Ni alloy surface was formed on a substrate with high Pd catalyst coverage. In this study, the thick NiP (approximately 450 nm thick) deposit on the Sn-Pd catalyzed surface had several large-size grains, indicated by red arrows (Fig. 2. 3. 4e), resulting in a rougher NiP morphology. This is attributed to poorer Pd catalyst coverage on the Sn-Pd catalyzed substrate (Fig. 2. 3. 2c).

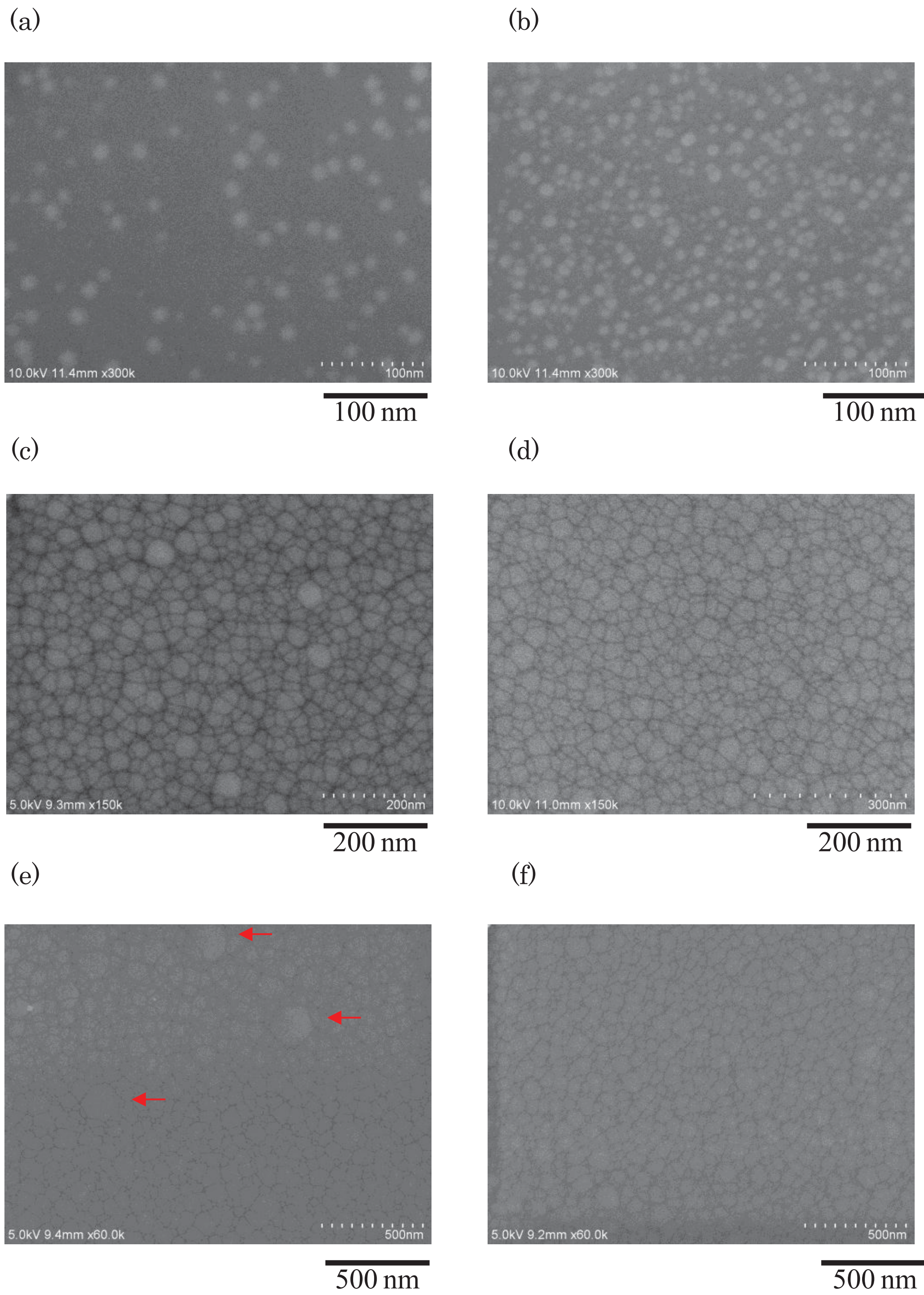

Fig. 2. 3. 4. FE-SEM images of electroless deposited NiP on flat SiO_2 substrate catalyzed by (a) (c) (e) Sn-Pd or (b) (d) (f) TAS-Pd. The NiP particles deposited within 30 s: (a), and (b). Thin NiP film: (c), and (d). Thick NiP film: (e) and (f).

2. 3. 4. The surface morphology of electroless deposited NiP on a trench-patterned master mold

NiP was uniformly and smoothly deposited on a trench-patterned master mold catalyzed by the TAS-Pd catalyzation process (Fig. 2. 3. 5b) due to high Pd catalyst coverage. In contrary, the NiP deposit on the Sn-Pd catalyzed master mold showed rough features (Fig. 2. 3. 5a) due to low Pd catalyst coverage. Based on the comparison of a NiP deposit on a Sn-Pd catalyzed flat substrate (Fig. 2. 3. 4c and e) and a Sn-Pd catalyzed trench-patterned master mold (Fig. 2. 3. 5a), the morphology of NiP on a trench-patterned master mold is even rougher, verifying low Pd catalysts coverage on 3D nanostructures. Nevertheless, the NiP deposit on a TAS-Pd catalyzed master mold (Fig. 2. 3. 5b) is as smooth as that on the flat substrate (Fig. 2. 3. 4d and f), indicating no apparent decrease in Pd catalyst coverage, even on 3D nanostructures. Smooth and uniform growth of NiP can prevent void formation; therefore, we expect geometric nanostructures to demonstrate higher replication ability through the TAS-Pd catalyzation process.

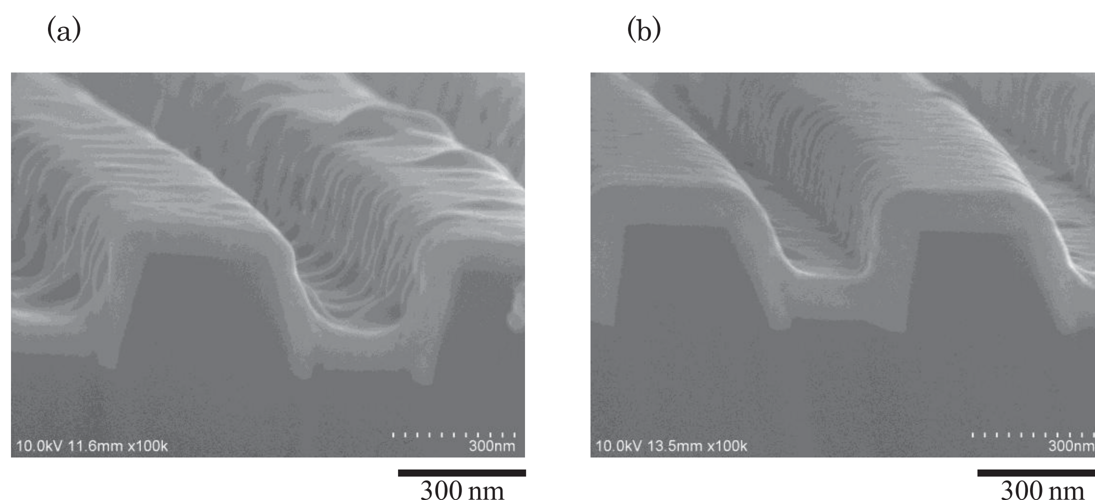

Fig. 2. 3. 5. FE-SEM images of electroless deposited NiP on trench-patterned master mold catalyzed by (a) Sn-Pd or (b) TAS-Pd catalyzation process

2. 3. 5. Adhesion strength between electroless deposited NiP and SiO_2 surface

Relatively lower adhesion strength between the electroless deposited NiP and the TAS-Pd catalyzed flat SiO_2 was confirmed (Fig. 2. 3. 6). In the present study, the adhesion strength of electroless deposited NiP to a Sn-Pd or TAS-Pd catalyzed flat SiO_2 substrate was investigated by a thin film mechanical property tester and each datum was averaged from five different points on a sample. In a thin film mechanical property tester, the inclined sample holder is set on a microbalance and an external force provided by a conical indenter with tip radius of 5 μm is applied to the sample (Fig. 2. 3. 7). When the sample is gradually pressed by the indenter, the measured weight will increase linearly with the external force. Once the external force exceeds the sum of the friction (FF) and the mechanical strength (FM), the film will be destroyed. The measured weight will fluctuate at the moment of destruction and the weight just before destruction is defined as the maximum applied load (Wmax). The adhesion strength investigated in the present work is estimated from the Wmax and the indentation depth at that moment [13]. In this study, the relatively lower adhesion strength between electroless deposited NiP and TAS-Pd catalyzed flat SiO_2 was attributed to the SAM as an interlayer to decrease the interface-friction between NiP and the SAM modified substrate [14]. Therefore, the force required to exceed the sum of interface-friction (between NiP and SAM modified substrate) and the mechanical strength of deposited NiP decreased, and the relatively lower adhesion strength was estimated. In contrary, the NiP deposited on Sn-Pd catalyzed substrate directly contact to the substrate, resulted in high interface-friction. Therefore, the force required exceeding the sum of interface-friction (between NiP and Sn modified substrate) and the mechanical strength of deposited NiP increased, and the relatively higher adhesion strength was estimated. Moreover, as the thickness of the NiP film increased to approximately 400–500 nm, the adhesion strength also slightly increased due to the higher mechanical strength of the NiP film. In Fig. 2. 3. 6, the positive deviation point of each adhesion strength datum is the maximum value within five different measured points on one sample. On the contrary, the negative deviation of each adhesion strength datum is the minimum value within five different measured points on one sample. As shown in Fig. 2. 3. 6, there is very little adhesion strength deviation among the five measured points for the NiP film on the TAS-Pd catalyzed substrate, which is attributed to the inherent uniform formation of SAM resulting in the uniform growth of NiP film. In other words, the properties of different points on the same NiP film should be almost the same. On the other hand, the high variation in adhesion strength values for the NiP film on the Sn-Pd catalyzed substrate implies non-uniform adhesion strength in the same NiP film. This explains why the electroless deposited

NiP on the Sn-Pd catalyzed master mold can only be completely detached in some areas (Fig. 2. 3. 8a and 9a).

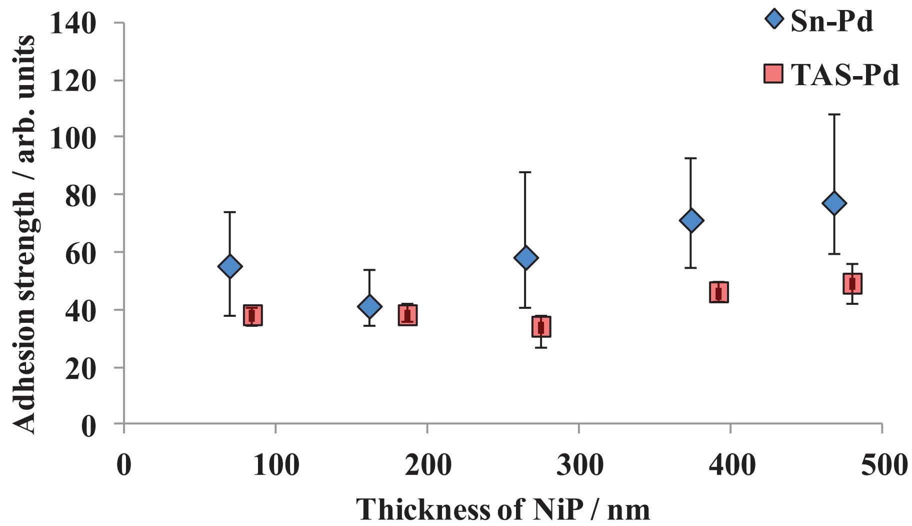

Fig. 2. 3. 6. Adhesion strength of electroless deposited NiP on flat SiO_2 substrate

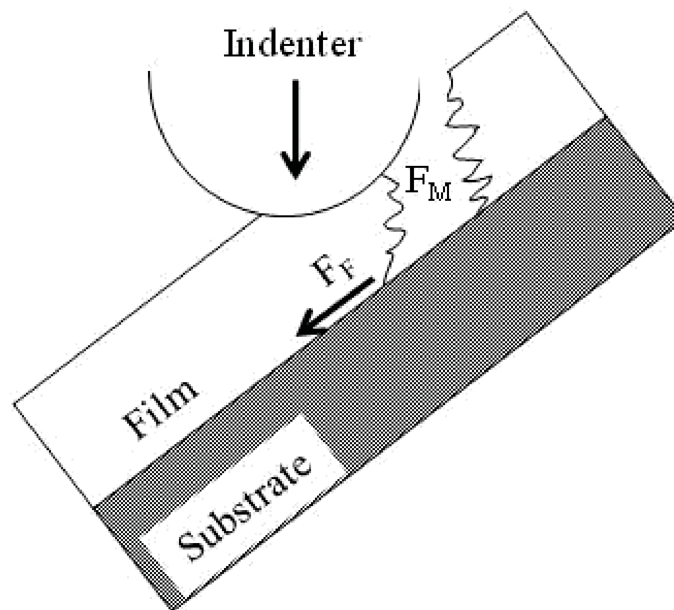

Fig. 2. 3. 7. Schematic illustration of thin film mechanical property tester

2. 3. 6. Replication of master mold

Electroless deposited NiP with a well-defined trench-patterned geometry was successfully detached from the TAS-Pd catalyzed master molds (Fig. 2. 3. 8b and d). The SAM (SAM: TAS) decreases adhesion strength between the electroless deposited NiP and master mold to an appropriate level, making it possible to smoothly detach the electroless deposited NiP from the master mold. Moreover, the well-defined nanopattern geometry can be replicated from the master mold, demonstrating the high replication ability of the master mold through SAM. On the contrary, high adhesion strength between the electroless deposited NiP and Sn-Pd catalyzed master mold results in broken NiP replicates and incomplete detachment. In other words, there are some unwanted defects formed on the surface of the detached NiP and the geometric nanopatterns of the master mold cannot be fully replicated (Fig. 2. 3. 8a and c).

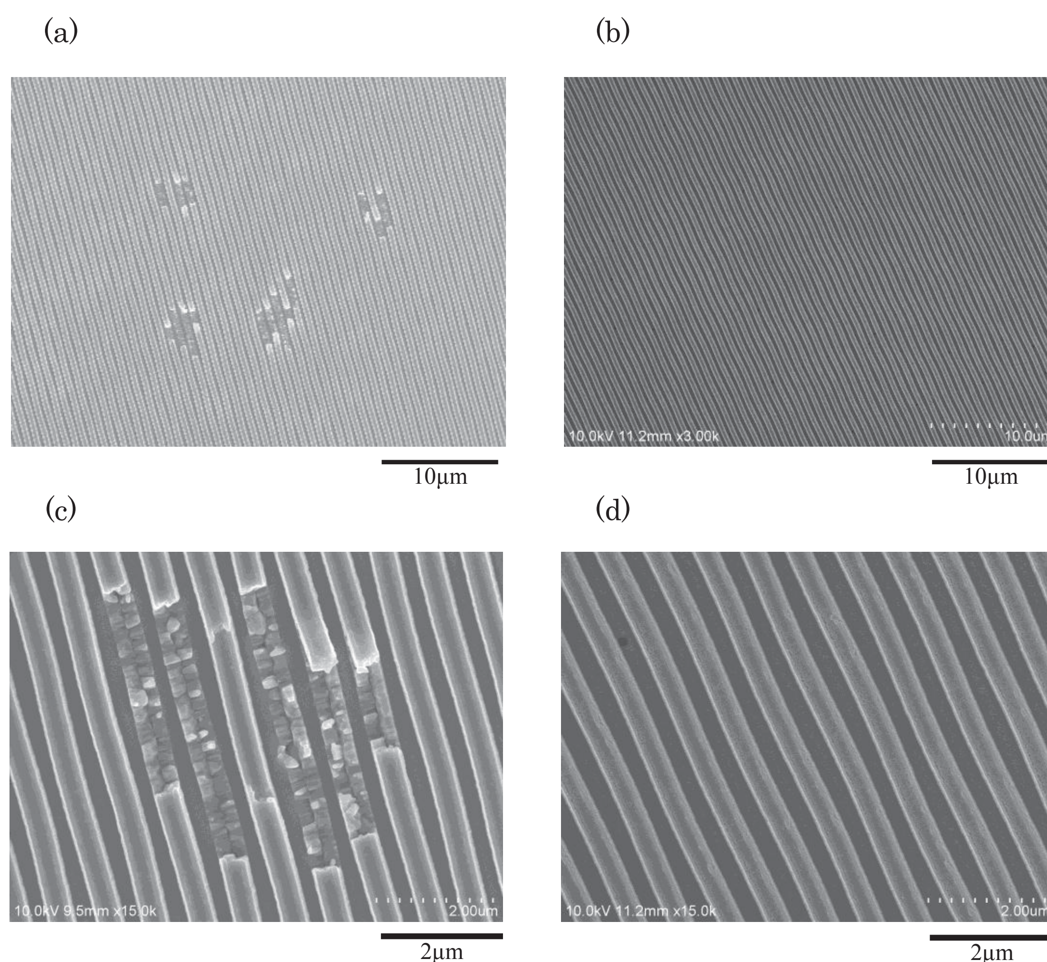

Fig. 2. 3. 8. FE-SEM images of electroless deposited NiP detached from Sn-Pd [(a) and (c)] or TAS-Pd [(b) and (d)] catalyzed trench-patterned master mold.

The similar results could be achieved by using dot-patterned master mold (Fig. 2. 3. 9b and d), indicating that the SAM was effective in the master mold replication process, including the master mold with different geometrical nanopattern shapes. In addition, the well-defined nanopattern geometry can be replicated from the master mold. Based on the AFM results (not shown here), the nanodot-patterns of the detached NiP are approximately 200 nm in height, which is the same as the depth of the nanodot-patterns on the master mold. This result verifies that the nanodot-pattern geometry was completely replicated, demonstrating the high replication ability of the master mold through SAM. On the contrary, high adhesion strength between the electroless deposited NiP and Sn-Pd catalyzed master mold results in broken NiP replicates and incomplete detachment. In other words, there are some unwanted defects formed on the surface of the detached NiP (Fig. 2. 3. 9a and c) and the geometric nanopatterns of the master mold cannot be fully replicated.

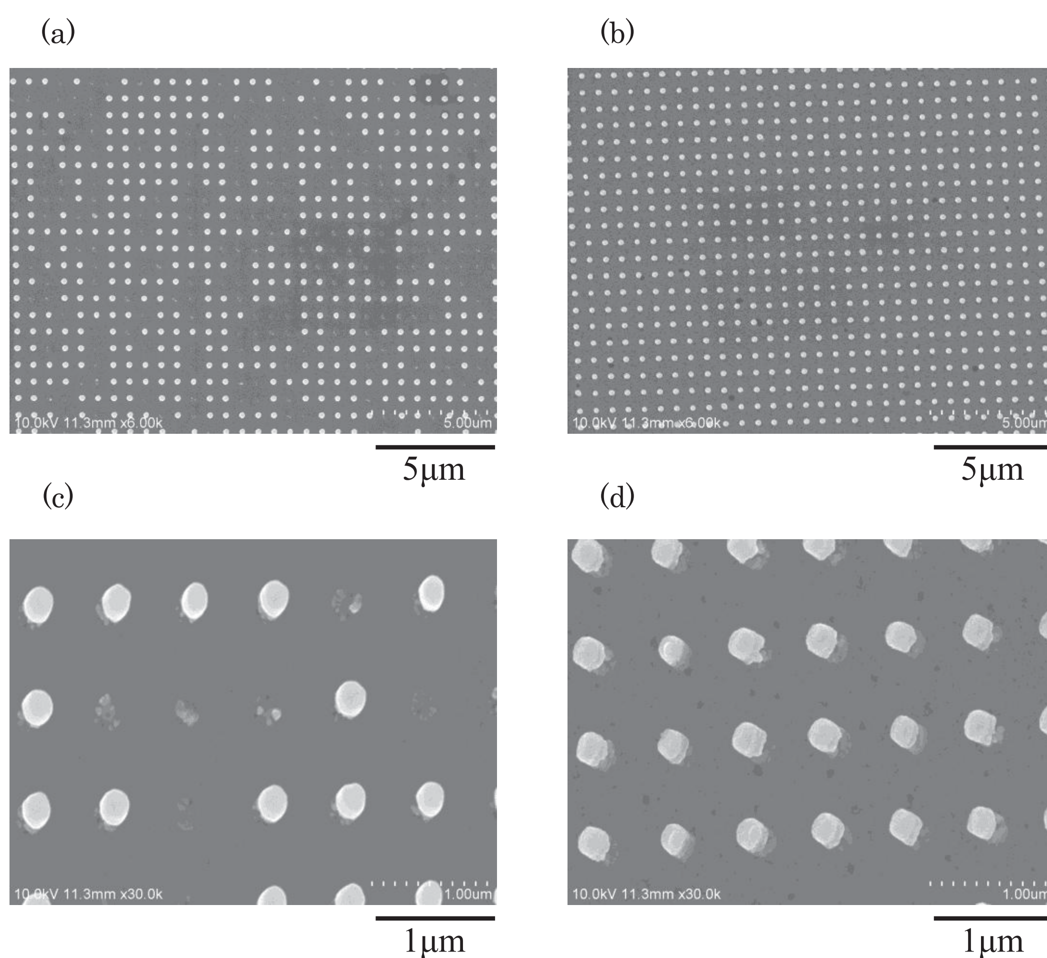

Fig. 2. 3. 9. FE-SEM images of electroless deposited NiP detached from Sn-Pd [(a) and (c)] or TAS-Pd [(b) and (d)] catalyzed dot-patterned master mold.

2. 3. 7. Sub-20 nm scale replication ability to master mold

Electroless deposited NiP with sub-20 nm scale replication ability to master mold could be achieved by employing TAS was confirmed. In Fig. 2. 3. 10a, there were some inherent defects with scale under sub-20 nm (indicated by red arrows) could be observed in the spaces of master mold, and the lines of master mold showed smooth surface (indicated by yellow circle). In Fig. 2. 3. 10b, the relative geometry of defects (indicated by red arrows) could be observed on the lines of electroless deposited NiP which detached from the TAS-Pd catalyzed master mold. Furthermore, the spaces of the detached NiP showed smooth surface (indicated by yellow circle). These results indicate that the master mold almost completely copied even the geometry of sub-20 nm, verifying that the replication ability of sub-20 nm can be achieved by employing SAM (SAM: TAS).

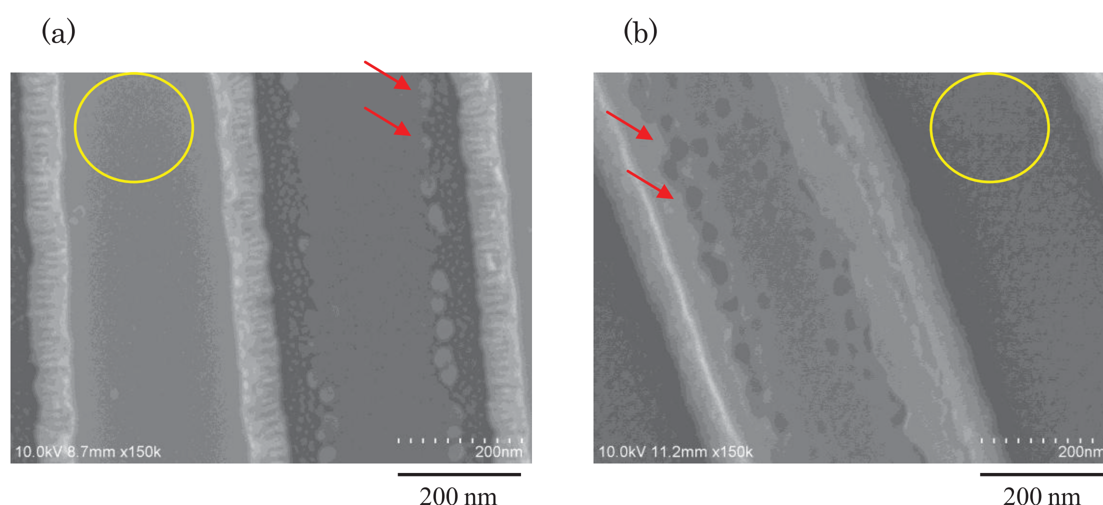

Fig. 2. 3. 10. FE-SEM images of (a) master mold and (b) electroless deposited NiP detached from TAS-Pd catalyzed master mold.

2. 3. 8. Conditions of self assembled monolayer after detachment

After detachment process, TAS remained on the surfaces of both master mold and detached NiP was confirmed. In this section, a flat SiO_2 substrate (without nanopatterns) was used to confirm the influences of detachment process on the TAS. The NiP was electrolessly deposited on a TAS-Pd catalyzed flat SiO_2 substrate, followed by detaching the deposited NiP from the flat SiO_2 substrate. The Auger mapping measurement was carried out on the surfaces of both SiO_2 substrate and detached NiP after detachment process. The AES mapping measurement of Si was carried out and the Si elements were observed on the surfaces of both SiO_2 substrate (Fig. 2. 3. 11a) and detached NiP (Fig. 2. 3. 11b). The Si element signals on the surface of detached NiP were considered coming from the TAS molecules. In addition, the AES mapping measurement of N element (which signal comes from the amino groups of TAS molecules) and Pd element (which signal comes from the Pd catalyst) were also carried out. The N elements were also observed on the surfaces of both SiO_2 substrate (Fig. 2. 3. 11c) and detached NiP (Fig. 2. 3. 11d). The SiO_2 substrate and detached NiP do not contain N elements, therefore the N element signals were considered coming from the amino groups of TAS molecules. The similar results could also been observed in the AES mapping measurement of Pd element (Fig. 2. 3. 11e and f). In addition, the non-uniform distribution of Si, N and Pd element on the surfaces of both SiO_2 substrate and detached NiP were observed, indicating that the TAS broke into pieces and partly remained on both surfaces after detachment (Fig. 2. 3. 12).

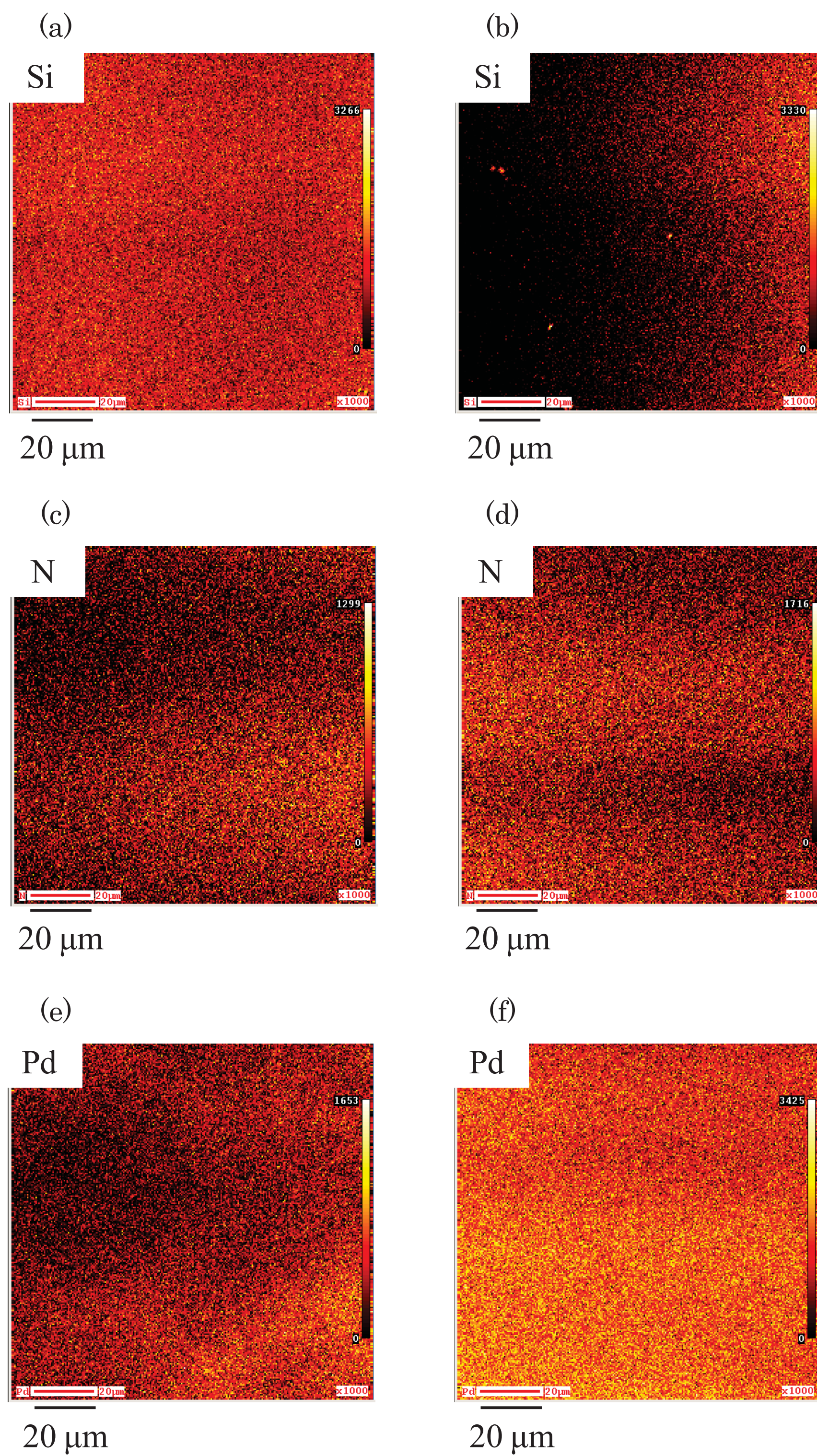

Fig. 2. 3. 11. AES mapping data of (a), (b) Si, (c), (d) N, and (e), (f) Pd elements on (a), (c), (e) flat SiO_2 substrate and (b), (d), (f) detached NiP after detachment.

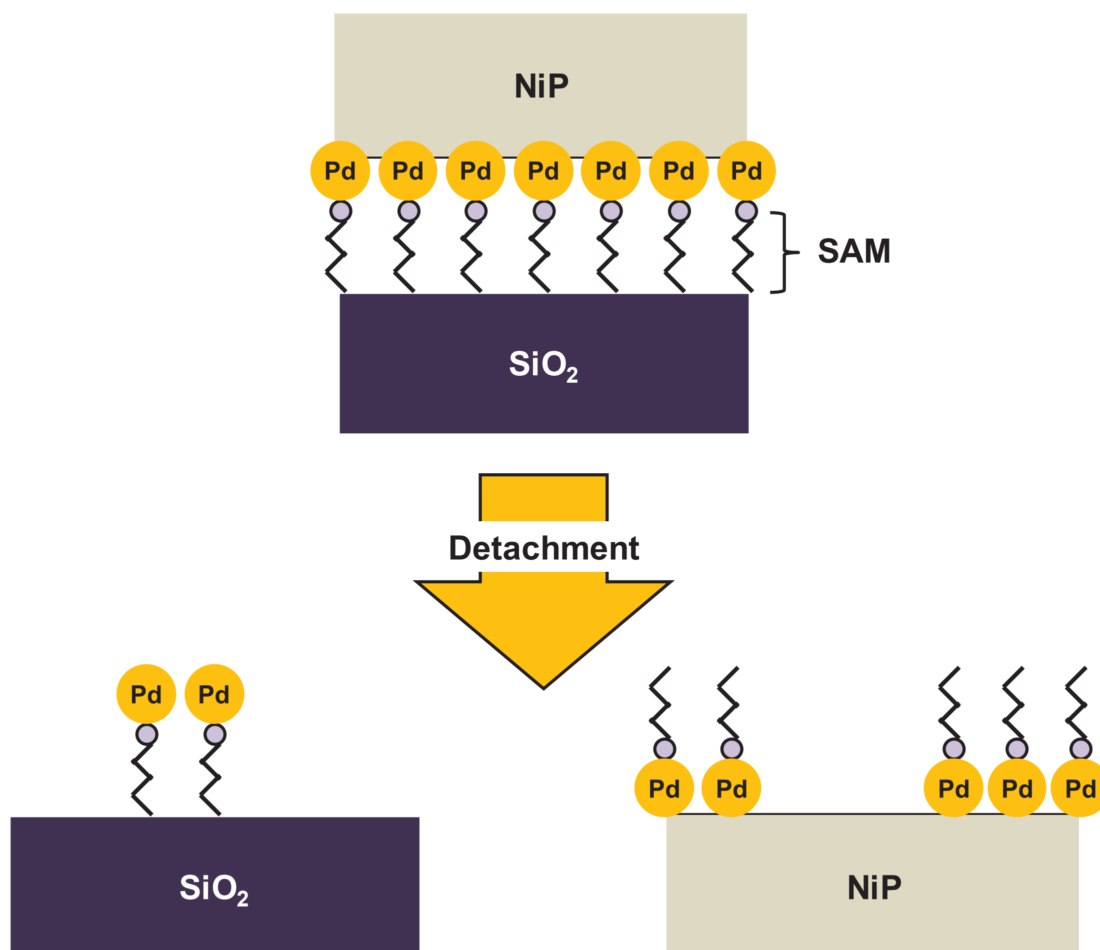

Fig. 2. 3. 12. Schematic illustration of SAM-Pd catalyzed SiO_2 surface and detached NiP surface after detachment.

2. 3. 9. Effect of self assembled monolayer on the adhesion strength

From section 2. 3. 1 to 2. 3. 6, comparisons between conventional Sn-Pd and SAM-Pd (SAM: TAS) catalyzation process were done, verifying the SAM effectively improve the Pd catalyst coverage, surface morphology of deposited NiP. Moreover, the adhesion strength between deposited NiP and master mold is control to an approximate level for smooth detachment. In this section, effects of amino group number of SAM are confirmed by a comparison of TAS, which possesses three amino groups in an individual molecule, and APTES, which possesses one amino group in an individual molecule.

The APTES-Pd catalyzed surface with fewer Pd catalysts than that on the TAS-Pd catalyzed surface was confirmed through GDOES measurement (Fig. 2. 3. 13). The intensity of Pd element in GDOES measurement is directly proportional to the amount of Pd catalyst. In other words, the lower the intensity of Pd element is, the fewer Pd catalysts exist. The lower intensity of Pd element observed on the APTES-catalyzed surface, indicating the APTES-Pd catalyzed surface with fewer Pd catalysts. In an individual APTES molecule, there is only one amino group used to coordinate with Pd ion, causing fewer amount of formation of Pd catalysts on the APTES-Pd catalyzed surface. In contrary, the three amino groups in an individual TAS molecule are supposed to strongly coordinate with one Pd ion, causing more amount of formation of Pd catalysts on the TAS-Pd catalyzed surface [10]. In addition, the Pd element signal was observed at the similar position (sputtering time) of Ni element signal, which originates from amino groups of SAM, on either TAS-Pd or APTES-Pd catalyzed surface, indicating the Pd element signal indeed comes from Pd catalyst, which coordinates with SAM.

The relative lower adhesion strength between deposited NiP and APTES-Pd catalyzed surface was confirmed (Table 2. 3. 1) and attributed to the following two reasons; (1) the fewer amount of Pd catalyst on APTES, and (2) the shorter chain length of APTES molecule. According the previous study [15-17], the adhesion strength between deposited alloy and substrate is directly proportional to the amount of Pd catalyst. Therefore, APTES-Pd catalyzed surface with fewer Pd catalysts is supposed as one of the reasons of relative lower adhesion strength between deposited NiP and APTES-Pd catalyzed surface. Besides the longer alkyl chains of TAS are much more flexible and can dissipate the external force [14] from the thin film mechanical property tester, resulting in the extra external force is needed to destroy the NiP film deposited on TAS (Fig. 2. 3. 7). Therefore, the relative higher adhesion strength between deposited NiP and TAS-Pd catalyzed surface was estimated.

Because of the lower adhesion strength is preferable for detachment; the APTES was mainly used hereafter in this thesis.

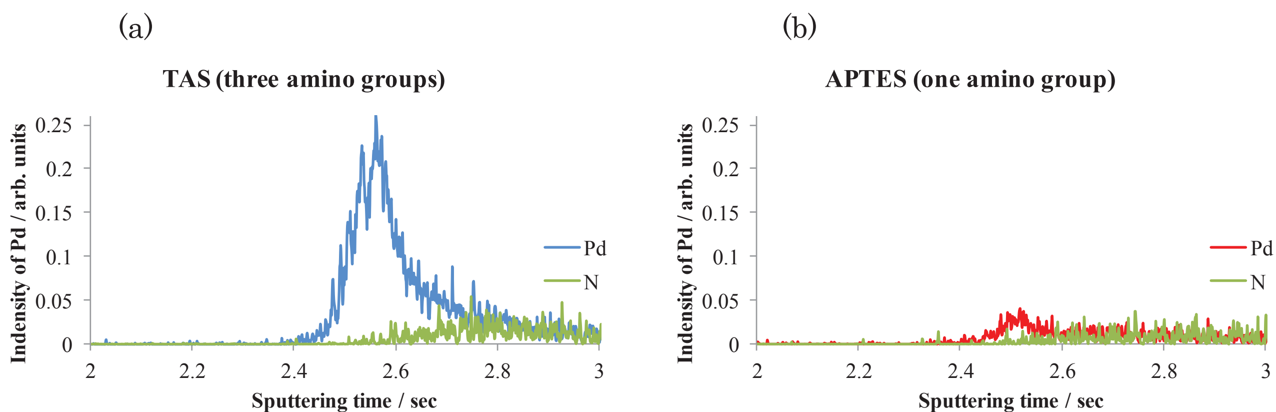

Fig. 2. 3. 13. GDOES measurement of Pd element on the (a) TAS-Pd or (b) APTES-Pd catalyzed surface.

Table 2. 3. 1

The adhesion strength of electroless deposited NiP on the TAS or APTES modified SiO_2 substrate

Catalyzation process	Adhesion (arb. Units)
TAS-Pd	38
APTES-Pd	31

2. 4. Conclusion

In chapter 2, the initial catalyzation conditions of SAM (SAM: TAS or APTES) catalyzation process were systematically investigated. The surface morphology of a catalyzed substrate was improved by applying the SAM. The SAM-Pd catalyzed substrate had higher Pd catalyst coverage than the Sn-Pd catalyzed substrate, resulting in the NiP electrolessly deposited on a SAM-Pd catalyzed substrate having a uniform and smooth morphology, even for a substrate with 3D nanostructures. Furthermore, the adhesion strength between the electroless deposited NiP and substrate was controlled to an approximate level by employing a SAM, which allows us to smoothly detach electroless deposited NiP from the master mold. In addition, the electroless NiP imprinting mold with nanometer-scale accuracy nanopatterns could be fabricated through a replication of a SAM-Pd catalyzed master mold was confirmed.

References

[1] A. N. Broers, A. C. F. Hoole, and J. M. Ryan, *Microelectron. J.*, **32**, 131 (1996).
[2] A. N. Broers, J. M. E. Harper, and W. W. Molzen, *Appl. Phys. Lett.*, **33**, 392 (1978).
[3] M. D. Austin, H. X. Ge, W. Wu, M. T. Li, Z. N. Yu, D. Wasserman, S. A. Lyon, and S. Y. Chou, *Appl. Phys. Lett.*, **84**, 5299 (2004).
[4] P. Palermo, A. Korpel, G. Dickinson, and W. Watson, Opt. Laser. Technol., **9**, 169 (1977)
[5] Y. Hirai, S. Harada, S. ISAKA, M. Kobayashi, and Y. Tanaka, *Jpn. J. Appl. Phys.*, **41**, 4186 (2002)
[6] S. Y. Chiu, J. M. Shieha, S. C. Chang, K. C. Lin, B. T. Dai, C. F. Chen, and M. S. Feng, *J. Vac. Sci. Technol. B*, **18**, 2835 (2000)
[7] M. Hasegawa, Y. Okinaka, Y. S.Diamand, and T. Osaka, *Electrochem. Solid-State Lett.*, **9**, C138 (2006)
[8] C. H. Lee, and T. P. Moffat, *Electrochim. Acta*, **55**, 8527 (2010)
[9] J. Han, J. Han, B. S. Lee, J. Lim, S. Kim, H. Kim, and S. Kang, *J. Micromech. Microeng.*, **22**, 065004 (2012)
[10] M. Yoshino, H. Aramaki, I. Matsuda, Y. Okinaka and T. Osaka, *Electrochem. Solid-State Lett.*, **12**, D19 (2009)
[11] S. L. Brandow, W. J. Dressick, C. R. K. Marrian, G. M. Chow, and J. M. Calverta, *J. Electrochem. Soc.*, **142**, 2233 (1995)
[12] T. K. Tsai, and C. G. Chao, *Appl. Surf. Sci.*, **233**, 180 (2004)
[13] Y. Tsukamoto, H. Kuroda, A, Sato and H. Yamaguchi, *Thin Solid Films*, **213**, 220 (1992)
[14] J. Ruehe, V. J. Novotny, K. K. Kanazawa, T. Clarke, and G. B. Street, *Langmuir*, **9,** 2383 (1993)
[15] T. G. Vargo, J. A. Gardella Jr., J. M. Calvert, and M. S. Chen, *Science*, **62**, 1711 (1993)
[16] M. Charbonnier, M. Alami, and M. Romand, *J Electrochem Soc*, **143**, 472 (1996)
[17] Y. Zhang, K. L. Tan, G. H. Yang, E. T. Kang, and K. G. Neoh, *J Electrochem Soc*, **148**, C574 (2001)

Chapter 3

Surface analysis of UV-treated cyclo olefin polymer for electroless NiP imprinting mold fabrication

3. 1. Introduction

In chapter 2, an electroless NiP imprinting mold with nanometer-scale accuracy was successfully fabricated through a replication of a SAM-modified inorganic master mold (made of SiO_2/Si).

Employing a polymeric plastic master mold to substitute the SiO_2/Si master mold is an alternative and potential candidate for further development of NIL mold fabrication due to the plastic raw materials with relatively low price and ease of processing. Moreover, the SAM can also be formed on the surface-pretreated polymeric plastic.

Generally, an OH-terminated surface is necessary for silane coupling reactions in order to form the silane SAM [1]. Therefore, an OH-group-free surface has to be modified for SAM formation. Osaka et al. used UV irradiation to modify the organic methyl silsesquioxane (MSQ) for generating −OH groups on its surface, and successfully formed a SAM on the MSQ surface, making the Ni alloy can be deposited on its surface (Fig. 3. 1. 1) [2].

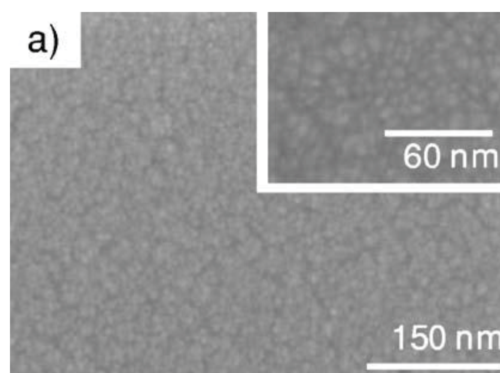

Fig. 3. 1. 1. The FE-SEM image of electroless NiB film on SAM-modified MSQ surface [2].

COP is increasingly applied as a substrate material due to its advantages such as high chemical resistance, sufficient strength and rigidity, and ease of processing [3]. Moreover, the surface properties (e.g., roughness, functional groups) of COP are controllable by UV irradiation treatment, such as −OH groups are generated (Fig. 3. 1. 2) [4-5]. The process, however, regarding the metallic mold fabrication by replication of a nanopatterned COP master mold has not been systematically studied yet.

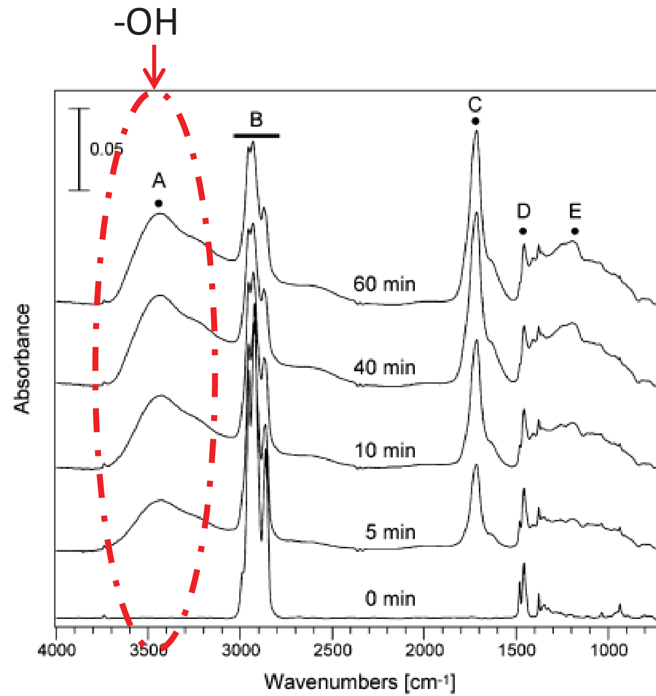

Fig. 3. 1. 2. FTIR-ATR spectra of COP surface: the –OH valence vibration peak can be observed after vacuum UV irradiation [5].

In this chapter, an electroless NiP imprinting mold was fabricated by replication of a COP master mold. By optimizing the UV irradiation time, the nanopattern geometry of the COP master mold was maintained. Moreover a SAM could be formed on the UV-modified COP surface to control the adhesion strength between the NiP deposit and the COP master mold to an appropriate level. This enabled smooth detachment of the NiP from the COP master mold.

3. 2. Experimental Methods

Substrate Clean:

The COP substrates (ZEON, ZEONOR) were rinsed in ethanol with ultrasonication for 10 min, followed by rinsing in deionized water (Milli-Q) prior to the UV irradiation treatment.

APTES-Pd Catalyzation Process:

APTES was formed on the UV-irradiation-treated COP substrate by immersing the substrate in an ethanol solution mixed with APTES (99 %, Aldrich Inc.) (Table 3. 2. 1) at 60 ° C for 10 min with subsequent rinsing in ethanol for another 10 min and ultrasonication to remove the excess amount of silane. The APTES formed substrate was then treated by Pd activation and DMAB solution as described in chapter 2

The experimental conditions and electroless deposition bath composition data are shown in table 3. 2. 3. A nanopatterned COP master mold was applied, which was fabricated by thermal imprinting process and provided by LEAP Co., Ltd (Fig. 3. 2. 1). The width and height of the nanopattern were approximately 100 nm and 70 nm, respectively. The NiP was electrolessly deposited on a UV-irradiation-treated and APTES-Pd modified COP master mold prior to Ni electrodeposition. The deposits (NiP and Ni) were finally detached from the COP master mold (Fig. 3. 2. 2).

The UV irradiation treatment was executed using a photo surface processor (SEN LIGHT, PL18-200). A low-pressure mercury lamp (SUV200GS-10), emitting UV light of wavelength 184.9 and 254.7 nm, was used. The distance between the lamp and the sample surface was approximately 10 mm. The water contact angle was measured from the LCD glass cleanness and treatment analyzer (KYOWA, LCD-400S). The surface morphology was observed by atomic force microscopy (AFM, BURKER, NanoScope IIIa) and field-emission scanning electron microscopy (FE-SEM, HITACHI, S-4800). The adhesion strength of the electroless deposited NiP to COP surface was investigated using a thin film mechanical properties tester (NEC, MH4000).

Table 3. 2. 1

The composition of APTES solution

Chemicals	Concentration
APTES	0.1 ml
Ethanol	10 ml
Temperature	60℃

Table 3. 2. 2

Compositions of electroless deposition solutions and experimental conditions

Chemical	Concentration (mol L^{-1})
CH_3COONH_4	0.4
$NiSO_4 \cdot 6H_2O$	0.1
$NaH_2PO_2 \cdot H_2O$	0.2
pH	4.5
Temperature	70 ° C

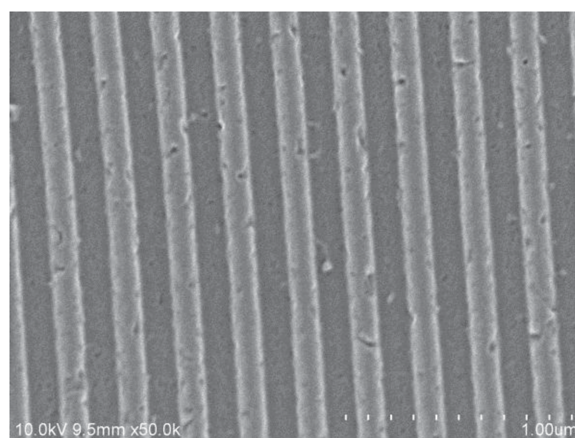

1 μm

Fig. 3. 2. 1. FE-SEM image of COP master mold.

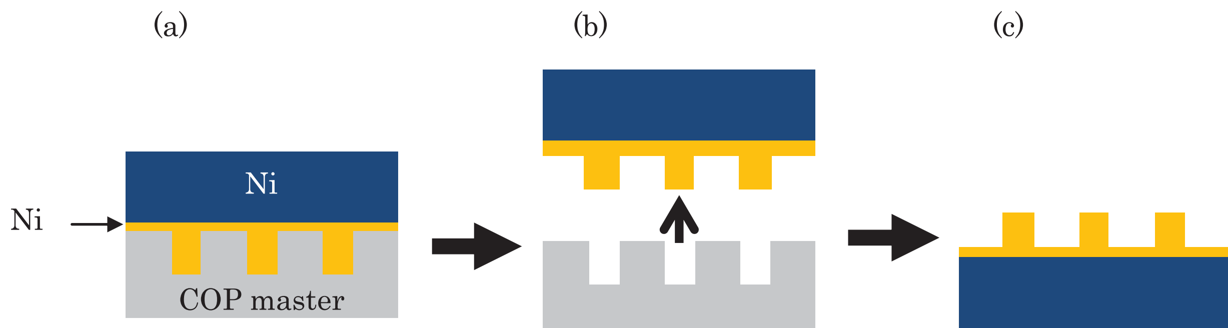

Fig. 3. 2. 2. Experimental processes: (a) NiP electrolessly deposited on an UV-irradiation-treated and APTES-Pd modified COP master mold prior to Ni electrodeposition (b) Deposit was detached from a COP master mold (c) Detached NiP with nanopatterns replicated from COP master mold.

3. 3. Results and Discussion

3. 3. 1. APTES formation on UV-irradiation-treated COP surface

Oxygen-containing functional groups (e.g., −OH) were generated on the COP surface after UV irradiation treatment for over 30 s confirmed by water contact angle measurement (Fig. 3. 3. 1a). The surface of the flat COP substrate was hydrophobic (water contact angle > 90 º) without any treatment. The water contact angle of a COP surface slightly decreased after UV irradiation for 10, 20, or 25 s, but the change was not distinct. In contrary, the water contact angle of a COP surface distinctly decreased after UV irradiation treatment for over 30 s (Fig. 3. 3. 1a), and this was attributed to oxygen-containing functional group formation, such as –OH groups [2, 4-5].

APTES was formed on the COP surface pretreated by UV irradiation for 30 s confirmed by water contact angle measurement (Fig. 3. 3. 1b). The APTES formation process was carried out on the UV-irradiation-treated COP surface, and the water contact angle was then investigated again. The water contact angles of 10, 20, or 25 s UV-irradiation-treated COP surfaces were not distinctly different after the APTES formation process, indicating that APTES did not form on the 10, 20, or 25 s UV-irradiation-treated COP surfaces. On the other hand, the water contact angle distinctly increased to 50-70° on the COP surface pretreated by UV irradiation for over 30 s was observed after the APTES formation process (Fig. 3. 3. 1b). The similar results could be observed by using the SiO_2 surface. The water contact angle on the piranha cleaned SiO_2 surface was below 30° but increased to higher than 55° on the APTES formed SiO_2 surface [6-8]. Therefore, the increases of water contact angle on COP surface pretreated by UV irradiation for over 30 s was supposed that the APTES was formed on the COP surface by a silane coupling reaction with the –OH group [2, 4-5]. In addition, the increase water contact angle on APTES formed COP surface was attributed to the amino-terminated surface (after APTES formation) which caused different surface energy to the hydroxyl-terminated surface (before APTES formation).

The electroless NiP deposition was then carried out on the COP substrates which were pretreated by UV-irradiation and APTES-Pd catalyzation processes successively. The NiP was almost not deposited on the 0, 10, 20, or 25 s UV-irradiation-treated and APTES-Pd modified COP substrates, verifying the APTES was not formed on the 10, 20, or 25 s UV-irradiation-treated COP surfaces. In contrary, a contiguous electroless NiP film could be deposited on the COP substrate, which pretreated by UV irradiation for over 30 s and APTES-Pd catalyzation process. This

result also suggested that the APTES was successfully formed on the COP substrate pretreated by UV irradiation for over 30 s for electroless NiP deposition.

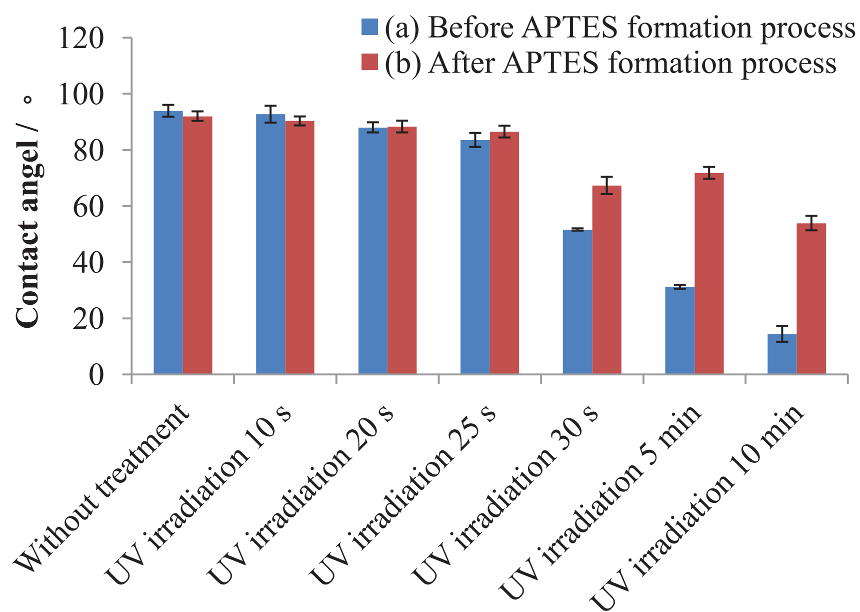

Fig. 3. 3. 1. Water contact angle measurement of COP surface (a) before APTES formation process and (b) after APTES formation process.

3. 3. 2. Optimization of UV irradiation treatment time

The average surface roughness (Ra) of the COP surface decreased with increasing exposure time to UV irradiation which was confirmed by AFM investigation. The Ra of a flat COP surface without UV irradiation treatment was 1.80 nm (Fig. 3. 3. 2a) and decreased to 0.59 and 0.30 nm after UV irradiation treatment for 5 and 10 min, respectively (Figs. 3. 3. 2b and c). Based on the AFM images, there were several defects easily observed on the surface of the COP substrate without UV irradiation treatment (Fig. 3. 3. 2a). Defects on the COP surface, however, were not apparent after UV irradiation treatment for 5 min (Fig. 3. 3. 2b). Furthermore, there were no distinct defects observed on the surface of the COP substrate after UV irradiation treatment for 10 min (Fig. 3. 3. 2c). This decrease in Ra and defects indicated that the COP surface was etched by the UV irradiation treatment [4-5].

The nanopattern geometry of a COP master mold was etched by UV irradiation treatment which corresponds to the AFM results. The nanopattern geometry of COP master mold was etched with increasing the UV irradiation period (Fig. 3. 3. 3), and there were almost no nanopatterns observed on the 10 min UV-irradiation-treated COP master mold (Fig. 3. 3. 3c). In contrary, the nanopatterns still maintain well geometric shape was observed on the COP master mold pretreated by UV irradiation for 30 s (Fig. 3. 3. 3a).

Based on the results of water contact angle measurements, electroless NiP deposition, AFM, and FE-SEM, APTES could be formed on a COP surface pretreated by UV irradiation for more than 30 s. However, nanopatterns of a COP master mold were etched with increasing exposure time to UV irradiation. Therefore, the optimum exposure time to UV irradiation was 30 s for the formation of APTES on COP surfaces and for preservation of the nanopatterns on the COP master mold. NiP electroless deposition was thus carried out on the COP master mold pretreated by UV irradiation for 30 s in subsequent experiments.

(a)

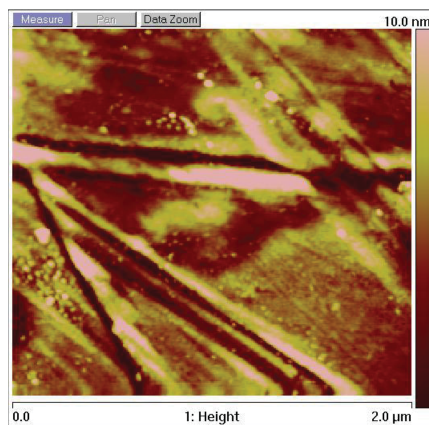

2 μm

(b)

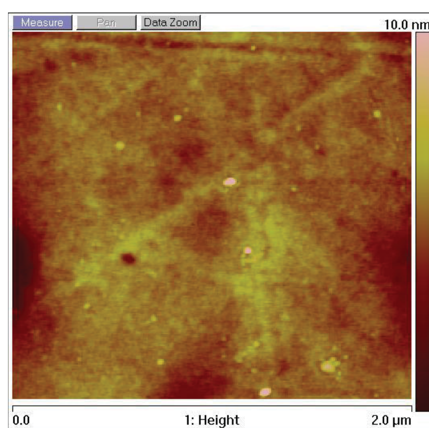

2 μm

(c)

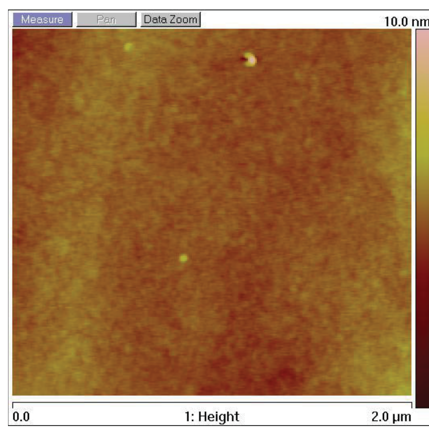

2 μm

Fig. 3. 3. 2. AFM images of COP surface pretreated by UV irradiation for (a) 0 min, (b) 5 min, and (c) 10 min; Z range = 10 nm.

(a)

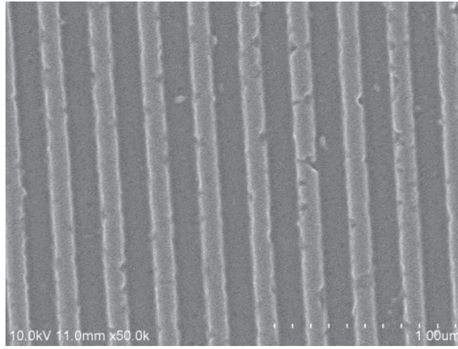

1 µm

(b)

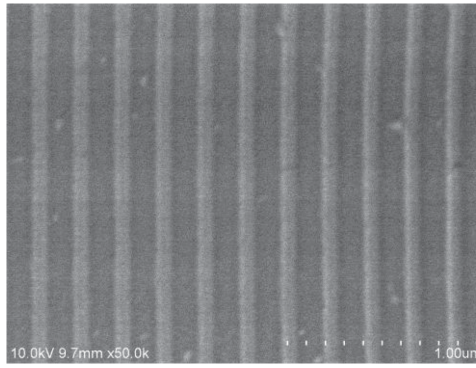

1 µm

(c)

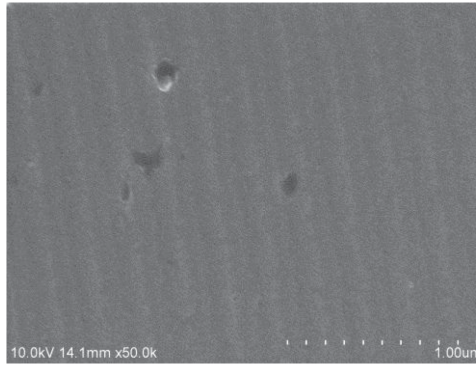

1 µm

Fig. 3. 3. 3. FE-SEM images of COP master molds pretreated by UV irradiation for (a) 30 s, (b) 5 min, and (c) 10 min.

3. 3. 3. Replicate mold

The electrolessly deposited NiP with well-defined nanopatterns was successfully detached from the UV-irradiation-pretreated and APTES-Pd modified COP master mold (Fig. 3. 3. 4). The width of space on 30 s UV-irradiation-treated COP master mold is approximately 160 nm (Fig. 3. 3. 3a), and width of line (replicated from the space of master mold) on the detached NiP is also approximately 160 nm (Fig. 3. 3. 4), there are no distinct difference was observed. In addition, some defects (few ten nanometer scale) on the COP master mold were observed, and the relative geometry of defects were also observed on the deposited NiP which was detached from the COP master mold. These results indicate that NiP replicate mold with high replication ability to COP master mold.

By optimizing the exposure time to UV irradiation, APTES could be formed on the COP master mold. Moreover, the adhesion strength between the electrolessly deposited NiP and pretreated COP substrate was close to a level of the well-known low adhesion strength between an Au film and SiO_2 surface [9] was confirmed. Furthermore, the damage to the nanopatterns of the COP master mold caused by overexposure to UV irradiation was minimized. Thus, an electroless NiP imprinting mold that could be fabricated by a replication of a polymeric master mold (COP in this these) was demonstrated.

*: The electroless NiP mold fabricated by using 5 min UV-irradiation-treated COP master mold was ever confirmed, and the result was shown in appendix 1.

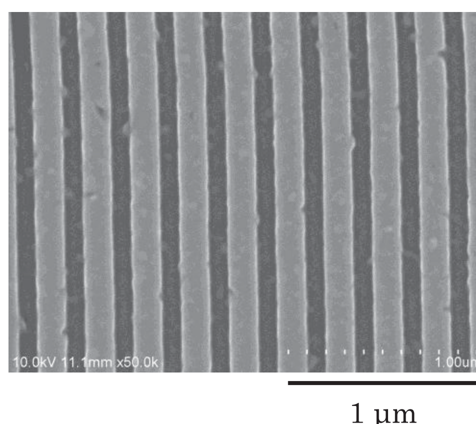

Fig. 3. 3. 4. FE-SEM images of the deposited NiP detached from 30 s UV-irradiation-treated COP master mold.

3. 4. Conclusion

APTES was successfully formed on a COP surface pretreated by UV irradiation for 30 s, allowing electroless NiP deposition on the COP substrate. In addition, the adhesion strength between deposited NiP and pretreated COP master mold was low enough, making an NiP with well-defined nanopatterns could be smoothly detached from the COP master mold. This chapter demonstrates that the electroless NiP imprinting mold can also be fabricated by a replication of an organic polymeric master mold, which modified with SAM.

Appendix

1. The electroless NiP imprinting mold fabricated by using 5 min UV-irradiation-treated COP master mold (used table 2. 2. 5. bath)

By using 5 min UV-irradiation-treated COP master mold, the electroless NiP imprinting mold with unwanted defects was observed (Fig. A1). Although the geometry of nanopattern of COP master mold was etched with increasing UV exposure time, it was still could find nanopatterns on the 5 min UV-irradiation-treated COP master mold (Fig. 3. 3. 3b). Therefore, we tried to use the 5 min UV-irradiation-treated COP master mold for electroless NiP imprinting mold fabrication. However, the deposited NiP could not be mechanically detached from the COP master mold, and it was need to use organic solvent (cyclohexane) to dissolve the COP master mold. The electroless NiP imprinting mold was then cleaned by acetone, followed by treating O_2 ashing plasma for ensuring there were no COP remained.

The unwanted defects were observed on the electroless NiP imprinting mold, and it was supposed that the overexposure UV irradiation not only etched the nanopatterns but also caused extra defects on the COP master mold, resulting in the NiP was deposited into such extra defects caused anchor effect. Therefore, the deposited NiP could not be mechanically detached from COP master mold as usual. Moreover, unwanted defects distinctly decreased the replication ability to COP master mold. In contrary, the deposited NiP with well-defined nanopatterns could be mechanically detached from the 30 s UV-irradiation-treated COP master mold (Fig. 3. 3. 4), demonstrating that the optimization time of UV irradiation is 30 s in this thesis.

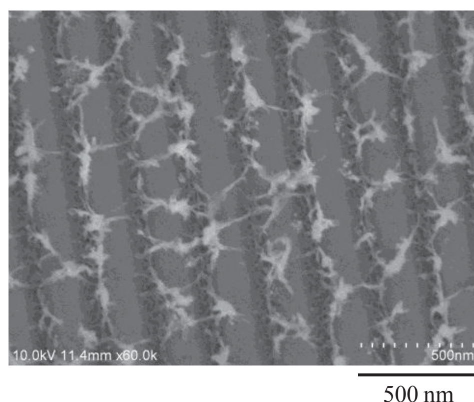

500 nm

Fig. A1. The FE-SEM image of NiP imprinting mold fabricated by using 5 min UV-irradiation-treated COP master mold.

References

[1] A. Ulman, *Chem. Rev.*, **96**, 1533 (1996)

[2] M. Yoshino, T. Masuda, T. Yokoshima, J. Sasano, Y. Shacham-Diamand, I. Matsuda, T. Osaka, Y. Hagiwara, and I. Sato, *J. Electrochem. Soc.*, **154**, D122 (2007).

[3] P. S. Nunes, P. D. Ohlsson, O. Ordeig, and J. P. Kutter, *Microfluid. Nanofluid.*, **9**, 145 (2010).

[4] H. Shinohara, J. Mizuno, and S. Shoji, *Sens. Actuators, A*, **165**, 124 (2011).

[5] Y. J. Kim, Y. Taniguchi, K. Murase, Y. Taguchi, and H. Sugimura, *Appl. Surf. Sci.*, **255**, 3648 (2009).

[6]S. Flink, F. C. J. M. van Veggel, and D. N. Reinhoudt, *J. Phys. Org. Chem*, **14**, 407 (2001).

[7] D. Janssen, R. D. Palma, S. Verlaak, P. Heremans, and W. Dehaen, *Thin Solid Films*, **515**, 1433 (2006).

[8] Y. Han, D. Mayer, A. Offenha¨usser, and S. Ingebrandt, *Thin Solid Films*, **510**, 175 (2006).

[9] M. A. Nicolet, *Thin Solid Films*, **52**, 415 (1978).

Chapter 4

Nanoindentation analysis for mechanical properties of electroless NiP imprinting mold

4. 1. Introduction

In chapter 2 and 3, an electroless NiP imprinting mold was successfully fabricated by a replication of either an inorganic (made of SiO_2/Si) master mold or an organic polymeric (COP) master mold.

For practical application of master mold replication in the NIL process, the accurate mechanical property analysis of a replicate mold (especially a singular nanopattern of a mold) is necessary. Mechanical property analysis especially in nanometer scale is demanded and studies by many researchers. Fang et al. [1] investigated the mechanical properties of vertical $(ZnO)_3In_2O_3$ nanowires and Wang et al. [2] investigated the mechanical properties of Ni nanodots by nanoindentation (Fig. 4. 1. 1). However, both of their investigation carried on more than one 3D nanostructures rather than a single 3D nanostructure in once investigation. Therefore the effects of interval between 3D nanostructures and mismatch of indenter and 3D nanostructures have been taken into account, resulting in complicated analysis of mechanical properties and reducing the reliability of results.

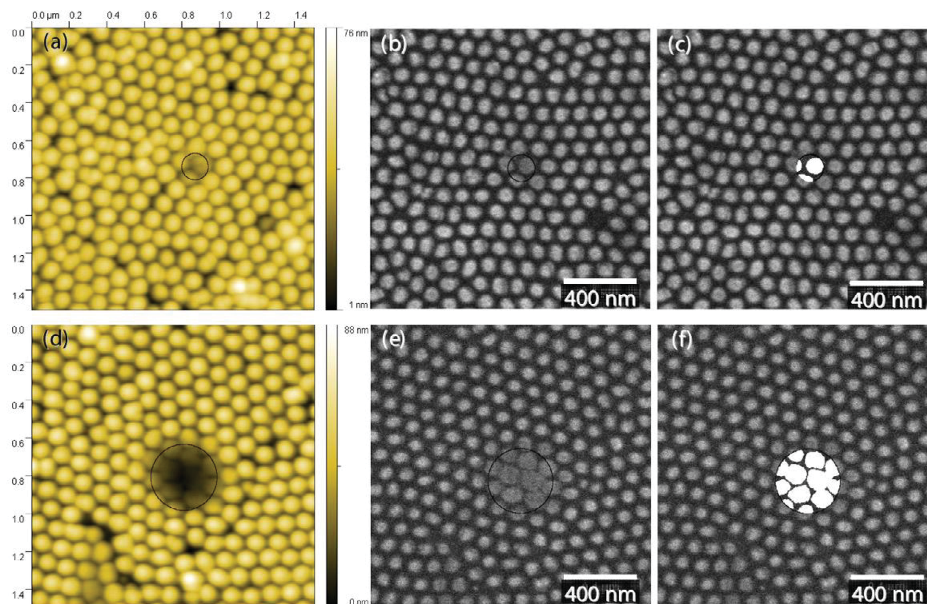

Fig. 4. 1. 1. Nanoindentation is carried out on Ni nanodots [2].

On the other hand, Ansari et al. [3] formed an electrodeposited Ni mold by the replication of a Si master mold and investigated its mechanical properties. However, they investigated the properties on the regions without nanopatterns. In other words, the mechanical properties of nanopatterns of Ni mold have not been investigated indeed. In general, the initial deposition conditions (e.g., grain size) of the Ni alloy are believed to affect the mechanical properties. Therefore, it is necessary to determine whether the different sizes of the nanopattern in the master mold affect the initial deposition conditions of the Ni alloy and further, the mechanical properties. However, the relation among the size of nanopattern of the master mold, the initial deposition conditions of the Ni alloy, and mechanical properties of the Ni alloy has not been systematically studied yet.

In this chapter, the amorphous (P = 9.85 wt%) NiP imprinting mold was fabricated by replication of a SiO_2 master mold, which had been formed nanopatterns with diameter of 170, 500, and 1000 nm on its surface. The initial deposition conditions of electroless NiP deposition in nanopattern of any size of master mold were investigated. In addition, the nanoindentation was precisely performed on a single nanopattern of NiP replicate mold for hardness investigation.

4. 2. Experimental Methods

Substrate Clean:

The SiO_2/Si substrate was rinsed in sulfuric peroxide mixture solution (SPM, H_2O_2:H_2SO_4 = 1:3) for 10 min, followed by rinsing in deionized water (Milli-Q) before the catalyzation processes and NiP electroless deposition.

APTES-Pd Catalyzation Process:

The detailed information is described in chapter 2.

The experimental conditions and electroless deposition bath composition data are shown in table 4. 2. 1. The SiO_2 master mold with nanopatterns of 170, 500, and 1000 nm was applied (Fig. 4. 2. 1), moreover, the height of each nanopattern is approximately 140 nm. The NiP was electrolessly deposited on an APTES-Pd modified SiO_2 master mold prior to Ni electrodeposition. The deposits (NiP and Ni) were finally detached from the SiO_2 master mold (Fig. 4. 2. 2).

Nanoindentation was performed on a single nanopattern of the detached NiP replicate mold for investigating the hardness using a method described by Miyake et al. (Fig. 4. 2. 3) [4]. The detailed information about nanoindentation probe and experiment was described in table 4. 2. 2. The probe (BRUKER, DNISP) is composed of a rectangular stainless steel cantilever and a three-sided pyramid diamond tip. The length, width and thickness of the cantilever are approximately 350, 100, 13 μm, respectively. Cantilever sensitivity was confirmed by using a sapphire sample before each nanoindentation experiment. For accurate measurement, the diamond tip was cleaned and the shape of tip was confirmed by performing nanoindentation on a standard Au sample, obtained from the manufacturer, before each nanoindentation experiment.

Surface morphology was observed using atomic force microscope (AFM, BRUKER, Nanoscope V), and field emission scanning electron microscope (FE-SEM, HITACHI, S-4800). Nanoindentation was performed using an atomic force microscope (AFM, BRUKER, Nanoscope V). The crystal structure was investigated by X-ray diffraction (XRD, BRUKER, D8 Discover). The composition of the NiP was analyzed by inductively coupled plasma optical emission spectrometry (ICP-OES, Thermo Fisher Scientific, iCAP6500).

Table 4. 2. 1
Compositions of electroless deposition solution and experimental conditions.

Chemical	Concentration (mol L^{-1})
CH_3COONH_4	0.4
$NiSO_4 \cdot 6H_2O$	0.1
$NaH_2PO_2 \cdot H_2O$	0.2
pH	4.5 or 6.5
Temperature	70 °C

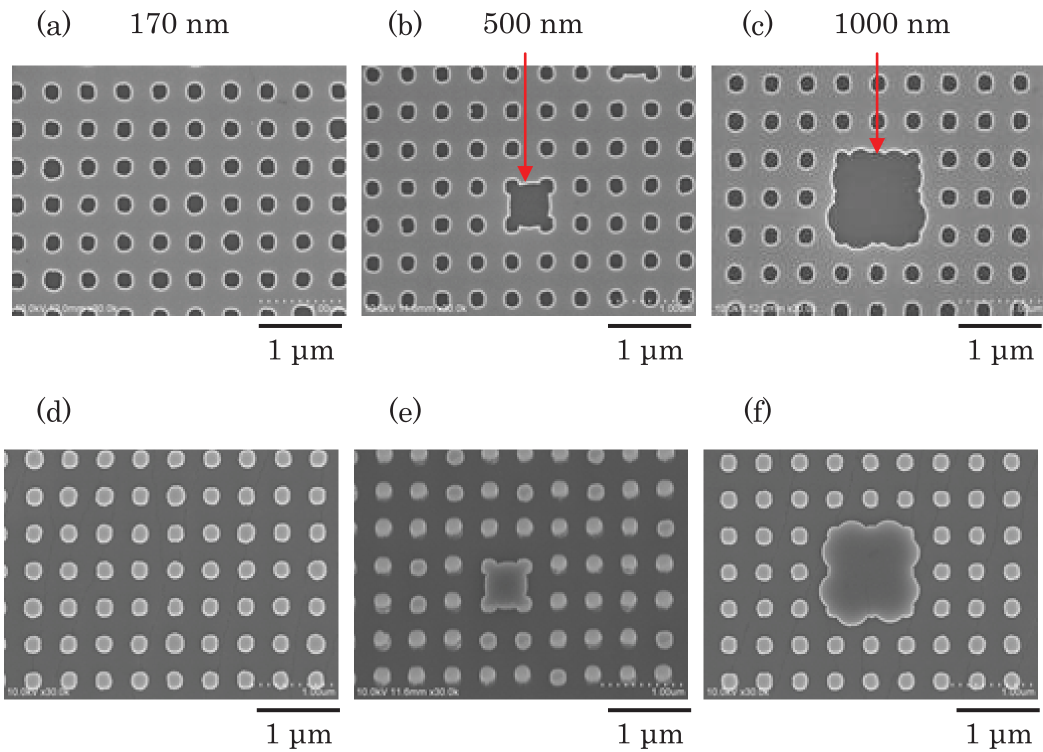

Fig. 4. 2. 1. FE-SEM images of master mold with nanopatterns of (a) 170 nm, (b) 500 nm, and (c) 1000 nm, and the corresponsive NiP replicate mold with nanopatterns of (d) 170 nm, (e) 500 nm, and (f) 1000 nm.

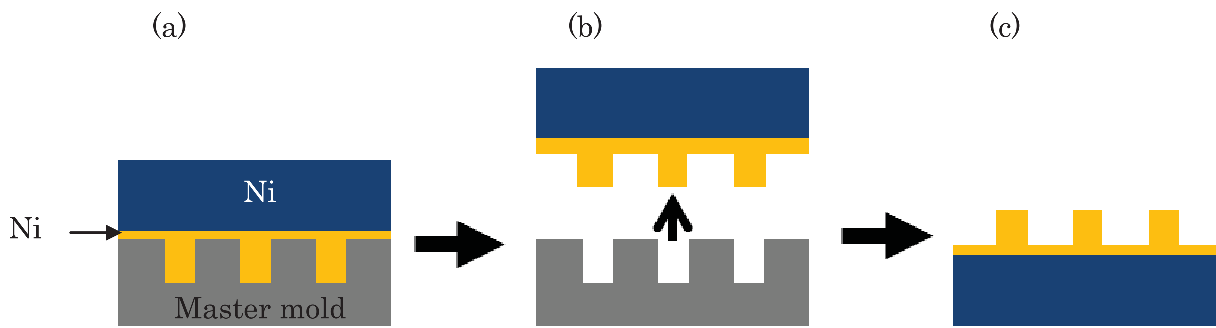

Fig. 4. 2. 2. Experimental processes: (a) Electroless deposition of NiP on an APTES-Pd modified master mold prior to Ni electrodeposition, (b) detached deposit from a master mold, and (c) detached NiP with nanopatterns replicated from the master mold.

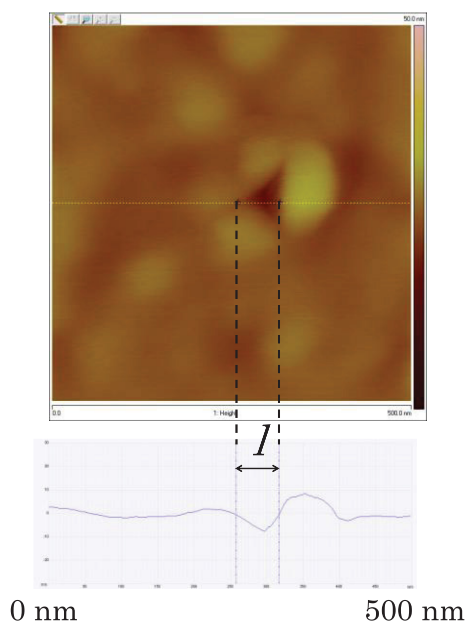

$$A_c = \frac{l^2}{\sqrt{3}\,\sin\alpha} \qquad H_{iAFM} = 1.74\,\frac{P_{max}}{A_c}$$

l : width of indent

α : Apical angle

A_c : Contact area

P_{max} : Applied force

H_{iAFM} : Hardness

Fig. 4. 2. 3. Schematic illustration of hardness analysis.

Table 4. 2. 2

Conditions of AFM nanoindentation

Probe	Three-sided pyramid diamond tip
Front abgel	55∘
Back angel	35∘
Tip Radius	40 - 50 nm
Spring constant	350 ± 35 N/m
X rotate	23∘
Applied force	20 - 60 μN

4. 3. Results and Discussion

Since the NiP was electrolessly deposited on a SiO_2 master mold and was then "detached" from the master mold (Fig. 4. 2. 2), it was necessary to confirm whether the properties of the detached NiP (NiP replicate mold), such as surface morphology and hardness, are the same as the as-deposited NiP. Moreover, the relation between the initial NiP deposition conditions in the nanopatterns of the master mold and the hardness of the NiP nanopatterns also needs to be investigated for ensuring that a NiP replicate mold with reliable properties is obtained. A detailed discussion of these investigations is described in the following sections

4. 3. 1. The crystal property of deposited NiP

The composition and crystal structure of the deposited NiP was investigated by ICP-OES and XRD measurements, respectively. In general, the NiP is amorphous when the P content is above 8 wt% and crystalline, when the P content is below 7 wt% [5]. In this study, the P content in the deposited NiP was 9.85 wt%, moreover, the Ni (111) peak was not observed (Fig. 4. 3. 1, red line). Therefore, the NiP was considered amorphous and used in subsequent experiments. In general, the amorphous NiP has better corrosion resistance, which may provide the imprinting mold with better durability and retention of the geometric shape of nanopatterns.

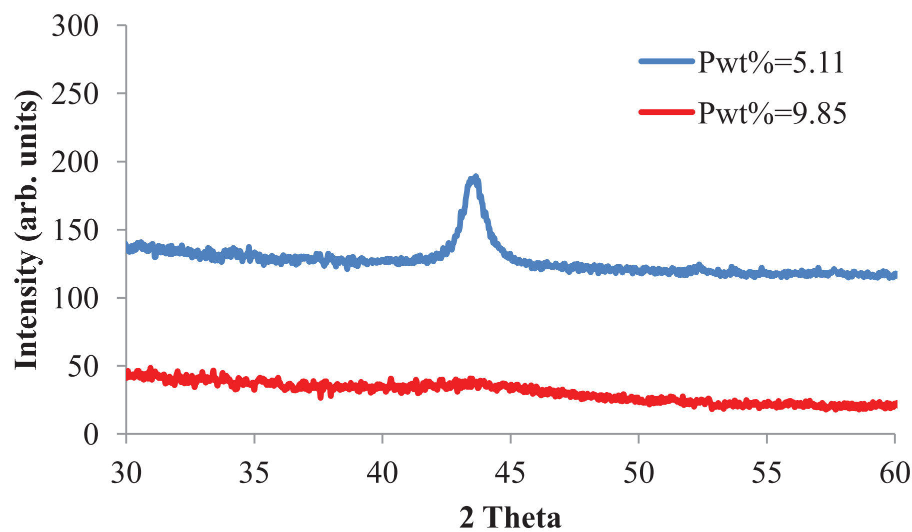

Fig. 4. 3. 1. The XRD spectrum of deposited NiP.

4. 3. 2. The surface morphology of as-deposited NiP and detached NiP

The surface morphology of the detached NiP (which was originally the interface between the deposited NiP and substrate but became the surface after detachment) showed lower surface roughness (Ra) and smaller NiP aggregates (Fig. 4. 3. 2b). The Ra of the detached NiP was 0.393 nm, which was lower than that of the as-deposited NiP (Ra = 1.19 nm). Moreover, smaller NiP aggregates were observed on the surface of the detached NiP. The lower Ra and smaller NiP aggregates are generally observed on the surface during the initial stage of the NiP electroless deposition, and the Ra and the size of NiP aggregates increases with deposition time [6-7]. Therefore, it supposed that the surface of the detached NiP is still maintained during the initial stage of the NiP electroless deposition.

The as-deposited NiP and detached NiP had similar grain sizes (Fig. 4. 3. 2c and d). The larger NiP aggregates that were observed on the surface of the as-deposited NiP (Fig. 4. 3. 2a) were composed of several small NiP grains, as observed using high-magnification AFM measurements (Fig. 4. 3. 2c) (similar results were also observed in a previous study [6]). Furthermore, NiP grains with a similar size were also observed on the surface of the detached NiP (Fig. 4. 3. 2d).

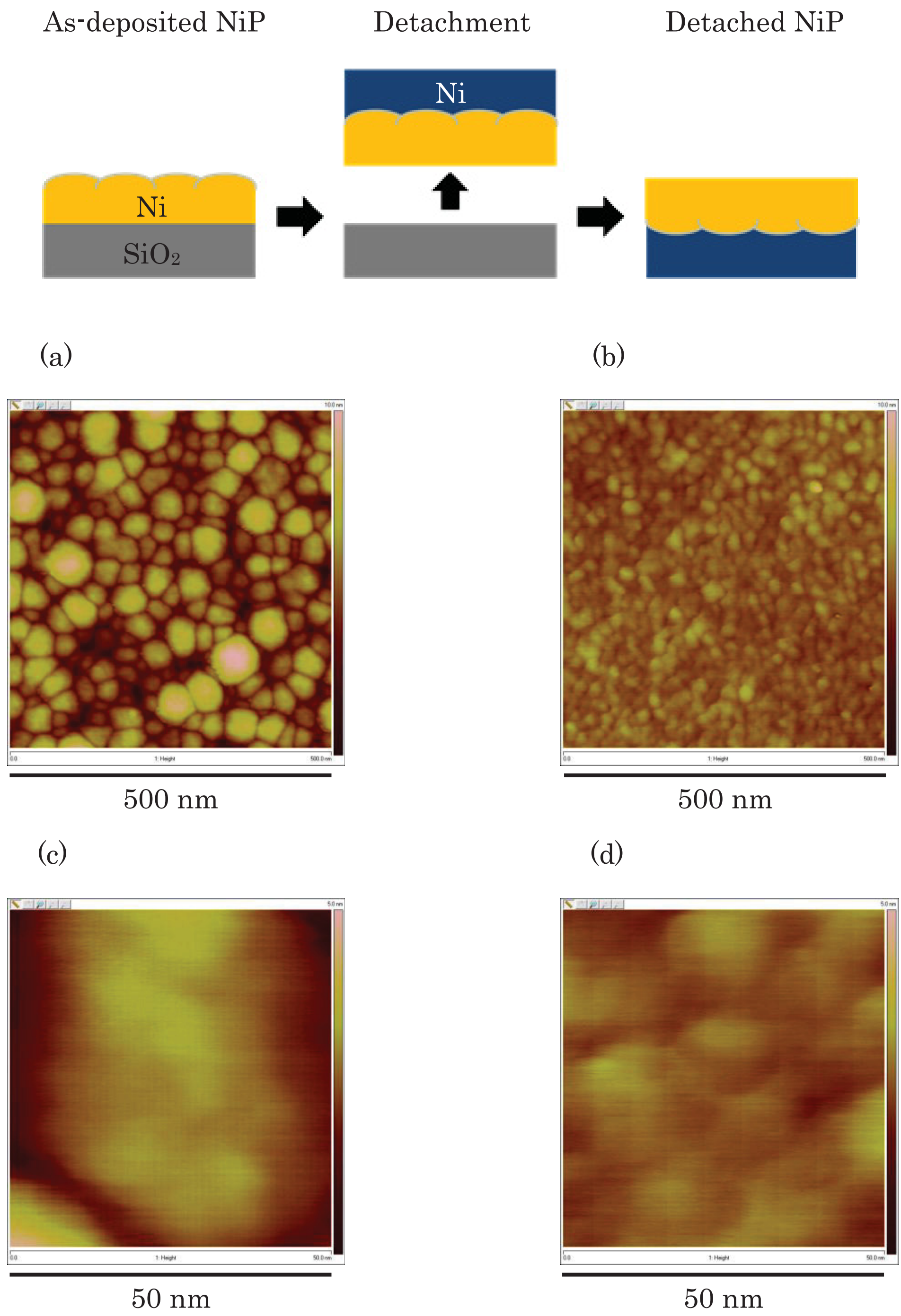

Fig. 4. 3. 2. Low-magnification AFM images of (a) as-deposited NiP and (b) detached NiP; Z range = 10 nm. High-magnification AFM images of (c) as-deposited NiP and (d) detached NiP; Z range = 5 nm.

4. 3. 3. The hardness of as-deposited NiP and detached NiP

It was determined that there is no effect of different substrates on the hardness of the as-deposited NiP and the detached NiP. To determine hardness, nanoindentation with various applied forces was carried out on the surfaces of both the as-deposited NiP and the detached NiP. As the substrate for the as-deposited NiP was SiO_2/Si, a hard material, and the substrate for the detached NiP was Ni, a soft material, it was necessary to confirm whether the hardness of NiP was affected by the different substrates. In general, the substrate effect on the hardness of the deposited film can be neglected when the indentation depth is less than one-fifth of the deposited film thickness [8]. In this study, all the depths of indentation were below one-fifth of the NiP film thickness (Fig. 4. 3. 3) (approximately 180 nm); therefore, the substrate effect on the hardness of NiP could be neglected.

The hardness of the as-deposited NiP and the detached NiP was similar (Fig. 4. 3. 4). Although the surface morphology and substrate of the as-deposited NiP and detached NiP were different (Fig. 4. 3. 2), a distinct difference in hardness of the as-deposited NiP and detached NiP was not observed. This was attributed to the fact that the as-deposited NiP and the detached NiP had similar grain sizes; moreover, the effect of the substrate on the hardness could be neglected. This suggests that the mechanical properties (hardness, in this study) of the electroless deposited NiP films were similar as long as the compositions (P content and NiP grain size, in this study) are the same, even though the surface morphologies are different. In addition, both the as-deposited NiP and detached NiP with a relatively higher hardness were observed in the case of nanoindentation with an applied force of 20 μN and this was attributed to the indentation size effect (ISE) [9]. ISE refers to the phenomenon where the hardness of the film increases with decreasing indentation depth and is generally observed when the indentation depth is less than approximately 5% of the film thickness [8]. When using an applied force of 20 μN, the indentation depth of the as-deposited and detached NiP were approximately 7% and 6% of the deposited NiP thickness, which is close to ISE limit of 5%. Therefore, the ISE was assumed to exist and caused a relatively higher hardness.

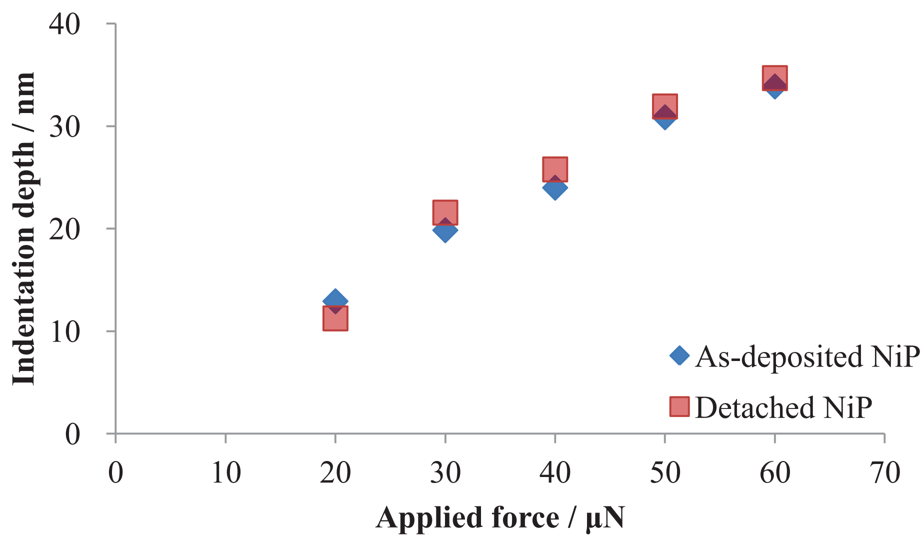

Fig. 4. 3. 3. The depth of indents of nanoindentation.

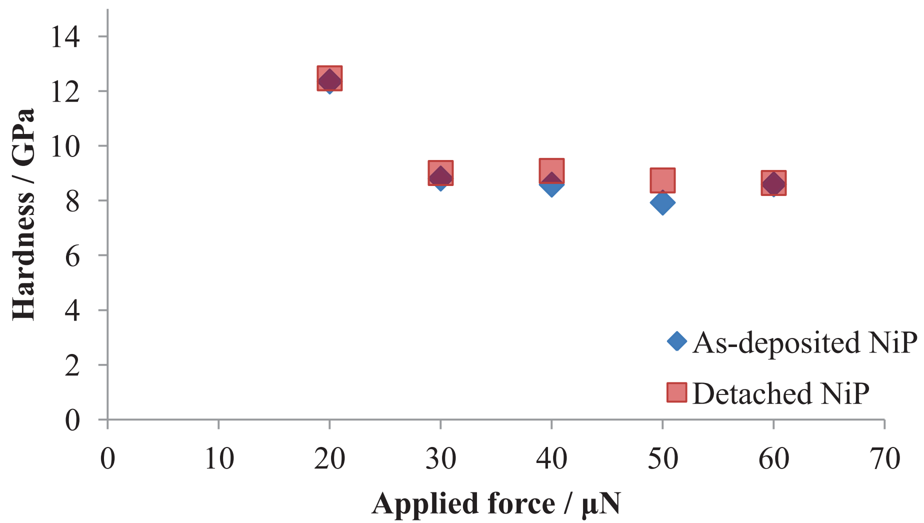

Fig. 4. 3. 4. The hardness of as-deposited NiP and detached NiP.

4. 3. 4. Initial deposition of NiP in various sizes nanopattern of master mold

That the initial deposition of NiP was not affected by the size of the nanopattern above 170 nm was demonstrated by observing the initial deposition in the nanopatterns of 170, 500, and 1000 nm, and the NiP grain size of 170, 500, and 1000 nm NiP nanopattern. The initial deposition condition (e.g., NiP grain size [10]) was considered to affects the mechanical properties of NiP. Therefore, it was necessary to investigate whether the different sizes of the nanopatterns of the master mold had any effect on the initial deposition condition of NiP. The NiP was electrolessly deposited into 170, 500, and 1000 nm nanopatterns for 10 s, and a NiP grain size approximately 10−15 nm in nanopatterns of any size was observed (Fig. 4. 3. 5).

Similar NiP grain size was observed across NiP nanopatterns of any size (Fig. 4. 3. 6). This was investigated by scanning the top surface of the nanopatterns. Small NiP grains were observed on the surface of NiP nanopatterns of any size, and a distinct difference in grain size was not observed (the reproducibility was checked by scanning other patterns), corresponding to the NiP initial deposition results (Fig. 4. 3. 5). The initial deposition of NiP was not affected by size of nanopattern above 170 nm.

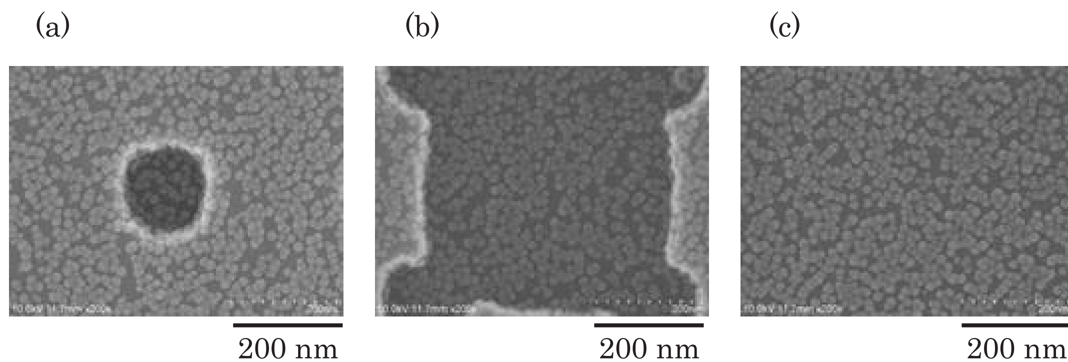

Fig. 4. 3. 5. The initial NiP electroless deposition in nanopattern of (a) 170 nm, (b) 500 nm, and (c) 1000 nm.

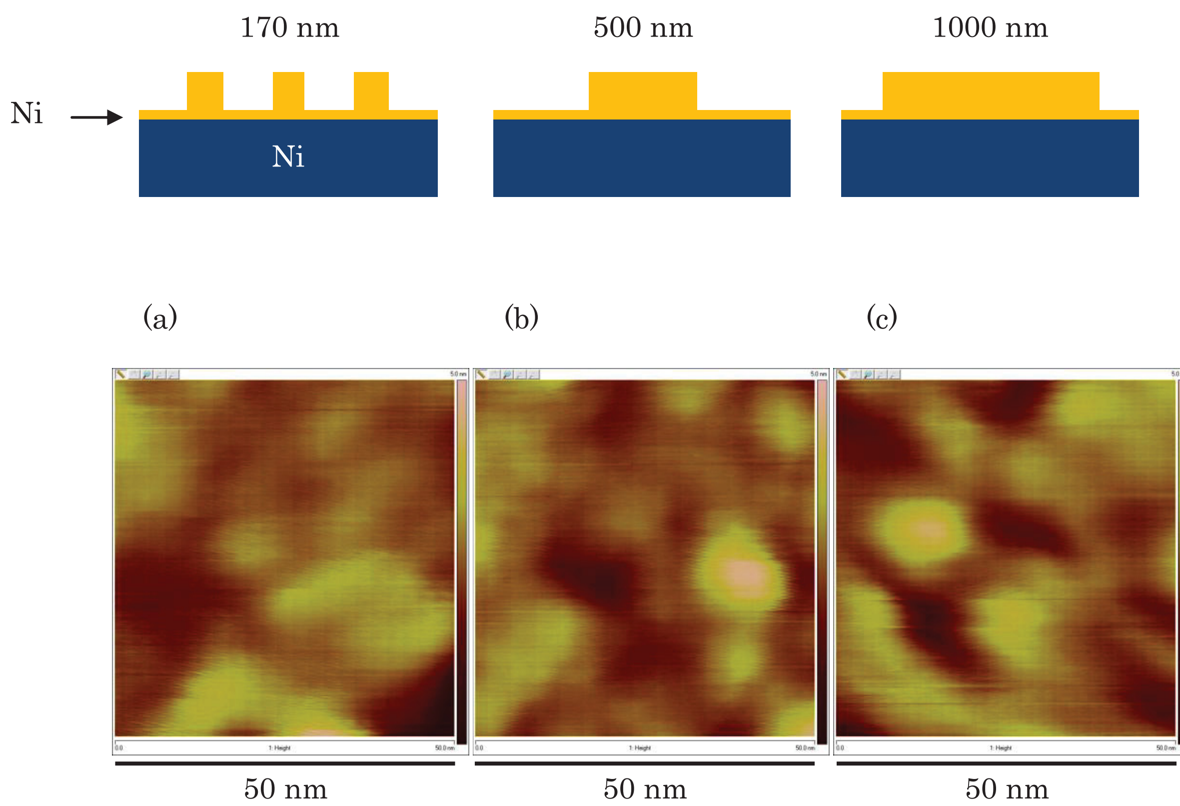

Fig. 4. 3. 6. The AFM images of NiP nanopattern of (a) 170 nm, (b) 500 nm, and (c) 1000 nm; Z range = 5 nm.

4. 3. 5. Nanoindentation analysis for mechanical property of various sizes NiP nanopattern

Nanoindentation was successfully performed on a single NiP nanopattern for investigating the hardness. The triangular indent observed (indicated by red arrows) on the NiP nanopattern after nanoindentation verified that the nanoindentation was successfully accomplished (Fig. 4. 3. 7). The applied force of nanoindentation was fixed at 20 μN, as a higher applied force tends to break apart the 170 nm NiP nanopattern. When a lower applied force was used, the triangular indent was difficult to form and distinguish on the NiP nanopatterns, resulting in a loss in accuracy of the measurement.

That the hardness of NiP was not size dependent above 170 nm was demonstrated by investigating the hardness of 170, 500, and 1000 nm NiP nanopatterns (Fig. 4. 3. 8). Each datum in Fig. 4. 3. 8 was an average of six results. In addition, a continuous NiP film was also investigated as a reference. There was no distinct difference in the hardness of NiP nanopatterns of any size, and a similar hardness was also observed on the continuous NiP film. The similar size of triangular indents on NiP nanopatterns (Fig. 4. 3. 7) also proved that the hardness of NiP nanopatterns of any size should be similar. The similarity of NiP during the initial deposition (Fig. 4. 3. 5) and similar NiP grain size (Fig. 4. 3. 6) in all sizes of the nanopattern were the reasons for a similar hardness of NiP. Furthermore, the hardness of NiP nanopatterns was approximately 12 GPa, which was relatively higher than the typical hardness of amorphous NiP (5-9 GPa [11-13]), due to ISE as described in Fig. 4. 3. 4. In other words, if there was no ISE, the real hardness of NiP nanopatterns is approximately 8−9 GPa (Fig. 4. 3. 4), which is of the same order as that of the general hardness of amorphous NiP. Ansari et al. [3] used a Ni imprinting mold, whose hardness is approximately 5 GPa, to successfully form nanopatterns on poly(methymethacrylate). Therefore, we conclude that the NiP imprinting mold fabricated in this study has a sufficient hardness to be employed in the NIL process.

The minimal size of nanopattern used in this work is 170 nm in diameter due to the inherent limitation of nanoindentation. For obtaining high accurate and reliable data of hardness of nanopattern, the nanoindentation has to perform on the center of a single nanopattern. However, the tip diameter (used in this work) of nanoindentation probe is approximately 100 nm which is close to the diameter of 170 nm nanopattern, resulting in the nanoindentation performing on the center of a single nanopattern with difficulty (the success rate is approximately 10 % in this work). The triangular indent of nanoindentation cannot be formed on the 170 nm nanopattern and the nanopattern is broken even though a slight misalignment. Therefore, the minimal size of

nanopattern used in this work is 170 nm for feasible experiment which is accurate and reliable.

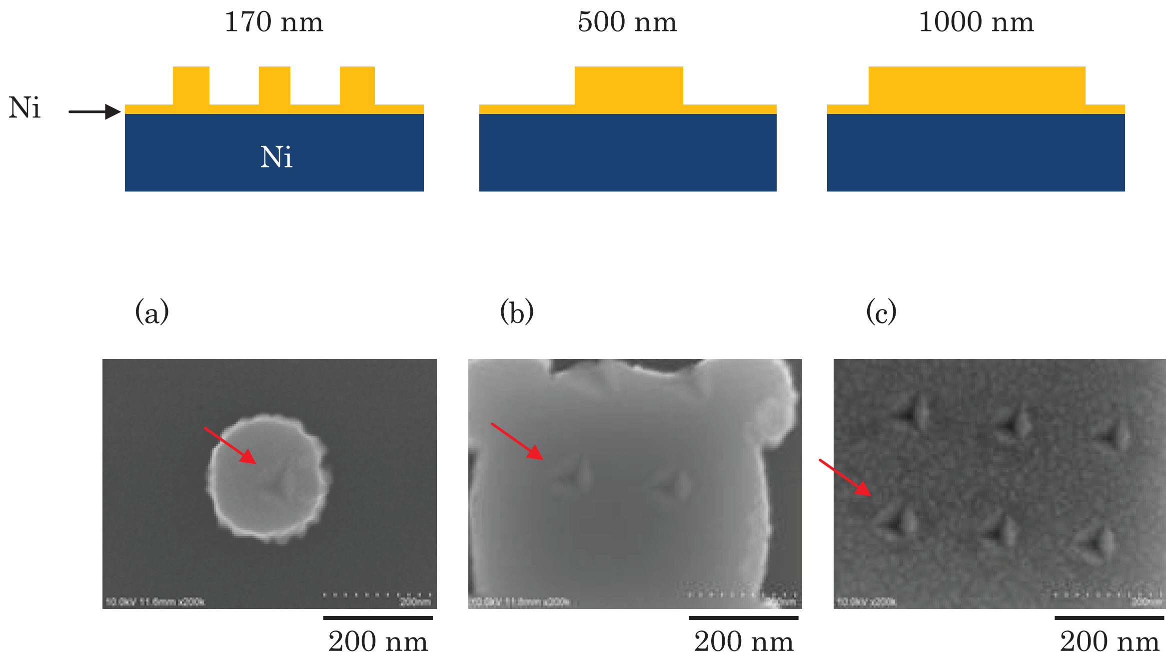

Fig. 4. 3. 7. The FE-SEM images of NiP nanopattern of (a) 170 nm, (b) 500 nm, and (c) 1000 nm after nanoindentation with applied force of 20 μN.

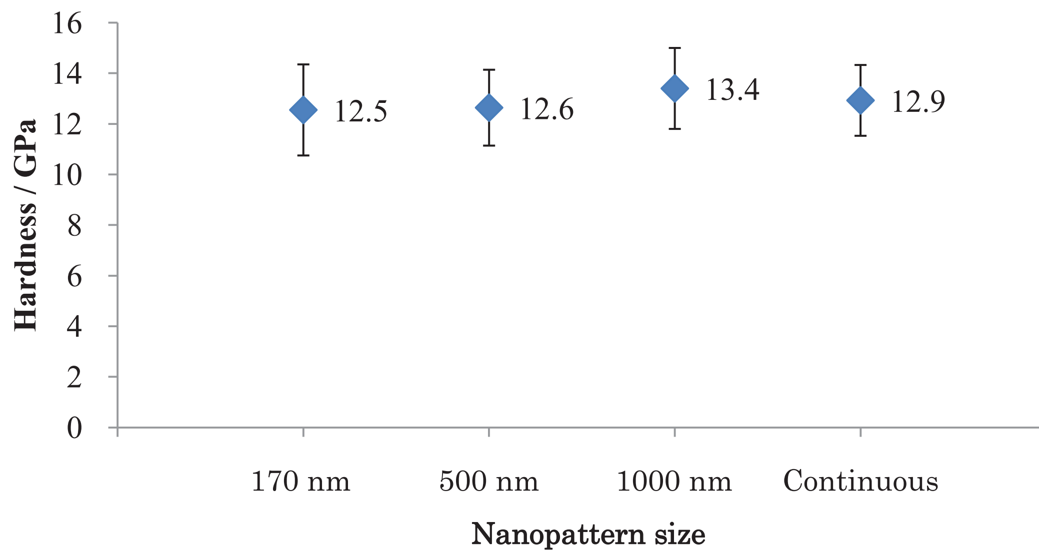

Fig. 4. 3. 8. The hardness of NiP nanopattern of 170 nm, 500 nm, and 1000 nm and continuous NiP film investigated by nanoindentation with applied force of 20 μN.

4. 4. Conclusion

The hardness of a single NiP nanopattern was successfully investigated by using nanoindentation. The initial NiP deposition condition and grain size of NiP were not affected by the size of nanopatterns above 170 nm. The hardness of 170, 500, and 1000 nm NiP nanopatterns and continuous NiP film were almost the same, indicating that the hardness of NiP was not size dependent above 170 nm. The experiments carried out in this study were also performed using crystalline NiP, and the results showed similar trends (not shown here), verifying the reproducibility of this study. The above results show that a NiP replicate mold with stable properties can be fabricated for application in NIL mold fabrication.

References

[1] T. H. Fang, and S. H. Kang, *J. Phys. D: Appl. Phys.*, **D 41,** 245303 (2008).
[2] H. Wang, M. Zou, P. R. Larson, E. S. Sanchez, K. L. Hobbs, M.E. Curtis, M. B. Johnson, and O. K. Awitor, *Nanotechnology*, **19**, 295708 (2008).
[3] K. Ansari, J. A. van Kan, A. A. Bettiol, and F. Watt, *Appl. Phys. Lett.*, 85, 476 (2004).
[4] K. Miyake, S. Fujisawa, A. Korenaga, T. Ishida, and S. Sasaki, *Jpn. J. Appl. Phys.*, **43**, 4602 (2004).
[5] J.Y. Song, and Jin Yu, *Thin Solid Films*, **415**, 167 (2002).
[6] T. Homma, M. Tanabe, K. Itakura, and T. Osaka, *J. Electrochem. Soc.*, **144**, 4123 (1997).
[7] T. K. Tsai, and C. G. Chao, *Appl. Surf. Sci.*, **233**, 180 (2004).
[8] R. Saha, and W. D. Nix, *Acta. Mater.*, **50**, 23 (2002).
[9] W. W. Gerberich, N. I. Tymiak, J. C. Grunlan, M. F. Horstemeyer, and M. I. Baskes, J. Appl. *Mech-T. Asme.*, **69**, 433 (2002).
[10] B. Yang, and H. Vehoff, *Acta. Mater.*, **55**, 849 (2007).
[11] B. Zhang, W. Wang, and G. P. Zhang, *Mater. Sci. Tech. Ser.*, **22**,734 (2006).
[12] P. Peeters, G.v.d. Hoorn, T. Daenen, A. Kurowski, and G. Staikov, *Electrochim. Acta*, **47**, 161 (2001).
[13] S.Y. Chang, Y. S. Lee, H. L. Hsiao, and T. K. Chang, *Metall. Mater. Trans. A*, **37A**, 2939 (2006).

Chapter 5

General Conclusion

This thesis had shown the feasibility of the combination of electroless deposition and SAM in NIL imprinting mold fabrication. The comparison between Sn-Pd catalyzation process and SAM-Pd catalyzation process was done and demonstrated that the SAM was effective in master mold replication process. As described in chapter 2, Pd catalyst coverage was improved by employing SAM, making the NiP could be uniformly deposited in nanopatterns of the SAM-Pd modified master mold to increase the replication ability. Moreover, the SAM allowed the adhesion strength between electroless deposited NiP and master mold tending to a level appropriate for smooth detachment. In general, the SAM is commonly used as adhesive layer between electrochemically deposited materials and substrate. In contrary, this thesis proved the SAM with capability to use as a lubricant but also maintained the geometry of deposited material (uniform deposition without peel off substrate). Furthermore, the adhesion strength was changed by using different types of SAM was confirmed and described in chapter 2. 3. 9. Such results suggest that the desired adhesion strength can be achieved by employing suitable types of SAM.

The electroless NiP imprinting mold with well-defined nanopattern could also be fabricated by a replication of UV-treated COP master mold was confirmed and described in chapter 3. This result verifies the SAM is also effective on organic polymeric surface. In addition, the geometry of nanopattern was etched due to overexposure of UV-irradiation was confirmed. If the exposure time of UV-irradiation can be adjusted in suitable period, the size of nanopattern of COP master mold is considered controllable, and beneficial for master mold replication process.

From the description in chapter 4, the surface morphology of detached NiP (replicate mold) was different from the as deposited NiP but the similar mechanical property tendency was observed. This phenomenon suggests that the mechanical property of electroless deposited NiP films should be the same as long as the compositions (P ratio and NiP grain size in this thesis) are the same, even though the surface morphologies are different. Moreover, it suggests that the detachment process does not affect the mechanical property of replicate mold.

The hardness of a single nanopattern of NiP imprinting mold was successfully investigated by nanoindentation, and demonstrated the NiP is not size dependent above the scale of 170 nm. In other words, the NiP nanopattern with the same property as bulk NiP material and suggests us that the replicate mold with reliable property can be applied in NIL process, further demonstrated that the SAM used master mold replication process with stability for application in NIL mold fabrication.

In this thesis, the fundamental researches in interfacial property had been systematically studied. By researching the interfacial properties, such as initial catalyzation, surface modification, initial deposition, the Ni alloy with desired properties, such as uniform surface morphology, appropriate adhesion strength to substrate, hardness could be formed. By taking advantage of these fundamental researches, a NIL imprinting mold with well-defined nanopatterns could be easily fabricated, and its mechanical property was precisely investigated. Basis on the results of this thesis, a large-area imprinting mold with accurate nanopattern can be fabricated with reliable property and low cost for practical application in NIL process was proposed.

Fig. 5. 1. Schematic illustration of this thesis.

Perspective

Through the fundamental research of interfacial properties, the electroless NiP imprinting mold with well-defined nanopatterns was successfully fabricated by a replication of either inorganic master mold or organic master mold in this thesis. There are still several topics need to be studied for making the electroless NiP imprinting mold more feasible in NIL process, and some of the author's opinions on NIL process are described as follows;

Surface roughness of nanopatterns of electroless NiP imptinting mold

The surface roughness of nanopatterns of imprinting mold is one of the key issues in the practical use of NIL process. The nanopatterns with rough surface make the additional applied force in imprint process is required. Moreover, the geometric shape of the patterned organic resist is deformed (Fig. 5. 2) in the detachment due to the high friction caused by rough surface of nanopatterns. It is necessary to study how to fabricate the low surface roughness imprinting mold for avoiding the unwanted defects on the patterned organic resist.

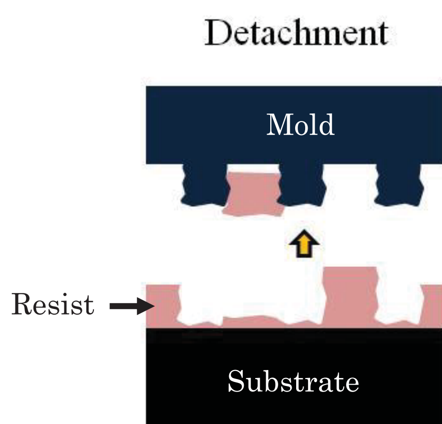

Fig. 5. 2. Schematic illustration of NIL process use imprinting mold whose surface is ronugh.

Flexibility of electroless NiP imptinting mold

The imprinting mold with flexible body and rigid nanopatterns is considered beneficial and important for the practical application in NIL. In the case of the organic

resist-coated substrate is slightly bended, even though the bend is in nanometer lengths, the nanopattern cannot be perfectly transferred on the organic resist due to the rigid imprinting mold does not completely fit the resist-coated substrate (Fig. 5. 3a), resulting in the decrease of resolution and reliability of NIL processes. On the other hand, the electroless NiP imptinting mold fabricated in this thesis is composed of flexible Ni body and rigid NiP nanopatterns, therefore, the electroless NiP imptinting mold can fit the resist-coated substrate for better pattern transfer. As a result, the high resolution and reliability NIL process may be achieved. However, the flexibility of imprinting mold is rare to be researched, it is necessary to study what is the appropriate flexibility for imprinting mold and its effects on the NIL process.

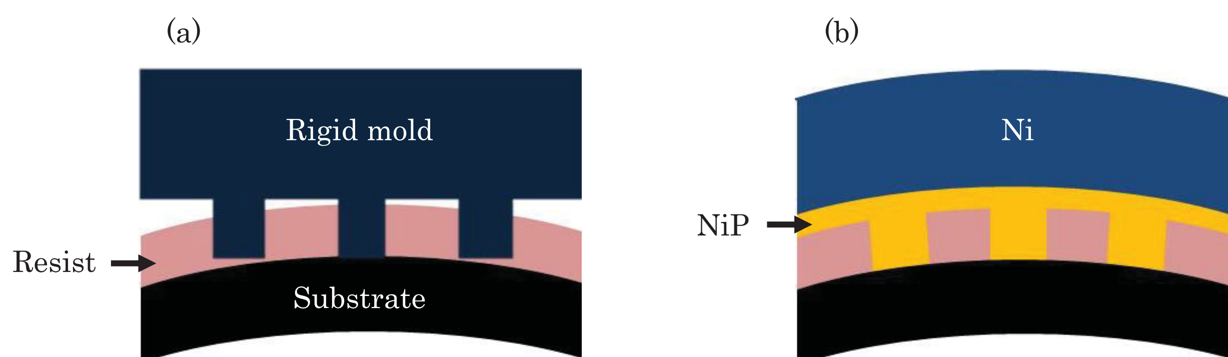

Fig. 5. 3. Schematic illustrations of (a) rigid mold or (b) flexible mold on a bending resist-coated substrate.

Appropriate nanopattern size of electroless NiP imprinting for practical applications

The author thinks the range of appropriate nanopattern size of imprinting mold is from few hundred nanometers to few micrometers, and the NIL process is especially expected to apply to microreactor, biotechnology, and optical elements. The imprinting mold whose patterns are few hundred nanometers or few micrometers is easily fabricated, and the problems caused by rough surface may be improved, in addition, the effects of small defects (few ten nanometers) on the performance of microreactor, or optical devices may be neglected due to different order of scale. On the other hand, as the nanopatterns of imprinting mold shrink to ultra small size ($<$ 50 nm), the effects of nanodefects or rough surface cannot be neglected, and the durability of imprinting mold may decreased. Those problems are harmful to the industrialization of NIL process.

List of Achievements

Original Article

"Initial catalyzation analysis of electroless NiP nanoimprinting mold replicated from self-assembled monolayer modified nanopatterns"
C. P. Lin, M. Saito, and T. Homma, *Electrochimica Acta*, **82**, 75 (2012)

"Fabrication of electroless NiP nanoimprinting mold by replication of UV-treated and self-assembled-monolayer-modified cyclo-olefin polymer nanopatterns"
C. P. Lin, M. Saito, and T. Homma, *Electrochemistry*, accepted

"Nanoindentation analysis for mechanical properties of electroless NiP imprinting mold replicated from self-assembled-monolayer modified master mold"
C. P. Lin, M. Saito, and T. Homma, *Jpn. J. Appl. Phys.*, submitted

Presentations

International Conference

"Fabrication and initial deposition analysis of electroless Ni alloy nanoimprinting mold replicated from SAM modified nanopatterns"
C. P. Lin, M. Saito, and T. Homma
62nd Annual Meeting of the International Society of Electrochemistry, Niitaga, September 2011

"Mechanical properties and initial deposition analysis of electroless Ni alloy nanoimprinting mold replicated from SAM modified nanopatterns"
C. P. Lin, M. Saito, and T. Homma
Joint Conference of The Fifth International Conference on the Science and Technology for Advanced Ceramics and The 2nd International Conference on Advanced Materials Development and Integration of Novel Structured Metallic and Inorganic Materials, Yokohama, June 2011

"Electroless-deposited NiP nanoarrays for nanoimprint replicated from a SiO2 mold"
C. P. Lin, M. Saito, J. B. Ratchford, and T. Homma
The 7th Asian Conference on Electrochemistry, Kumamoto, May 2010

Domestic Conference

"Nanoindentation analysis for mechanical properties of electroless NiP imprinting mold replicated from self-assembled monolayer modified patterns"
C. P. Lin, M. Saito, and T. Homma
2013 80th Spring Meeting of the Electrochemistry society of Japan, Sendai, Much 2013

"Fabrication of 80 nm-scale imprinting mold by detaching electroless-deposited NiP from SAM modified SiO_2 master mold"
C. P. Lin, M. Saito, and T. Homma
1st CSJChemistryFesta, Tokyo, November 2011

"Investigation on Mechanical Properties of Nanoimprint Mold Prepared by Electroless NiP with SAM"
C. P. Lin, M. Saito, F. Kitaoka, and T. Homma.
2010 77th Spring Meeting of the Electrochemistry society of Japan, Toyama, Much 2010

"Microstructural and mechanical properties of electroless NiP deposited at nano-patterned area"
C. P. Lin, M. Saito, and T. Homma
120th Annual Meeting of the Surface Finishing Society of Japan, Chiba, September 2009

Acknowledgement

First and foremost, I would like to express my sincere gratitude to my advisor, Professor. Takayuki Homma for his support, understanding and patience during the past five years. I learned not only the matters about academic researches, but also received a new view of life under Professor. Takayuki Homma's guidance. I really appreciate Professor. Takayuki Homma gave me the chance to study in Japan. The Japan's life experience is a priceless treasure and beneficial to my whole life.

I would also like to express my sincere gratitude to Professor. Tetsuya Osaka for sharing his life experiences to me and giving me a lot of edifications, valuable advices, and encouragements.

I would also like to express my sincere gratitude to Professor. Chi Chang Hu for taking his valuable time, and always encourages me, giving me a lot of valuable advices. I also really appreciate Professor. Chi Chang Hu gave me the chance to study in Japan and supported me as I felt struggle.

I would like to thank Professor Kazuyuki Kuroda, Professor Yoshiyuki Sugahara, and Professor Toshiyuki Momma for reviewing my thesis.

I also appreciate Professor. Mikiko Saito for her advices and the support to my research, and appreciate her for her concern. I also wish to express my appreciation to Professor. Yasuhiro Fukunaka for his encouragement at my first time Japanese presentation. I would like to thank Professor Masahiro Yanagisawa for teaching me how to use SERS.

I would like to thank Dr. Masahiro Kunimoto for his support and valuable advices and appreciate him that he always helps me as I need. I would like to thank all members of Homma group. It was so difficult to do my own research and live in Japan without your kind helps and advices. Special thanks to Mr. Yuki Arikawa for his friendship and support in the times that I needed it most in Japan. I also thank all my friends in both Japan and Taiwan for their support and friendship.

Lastly, I would like to thank my family for all their love, support, and encouragement. I really appreciate my parents who raised me with patience and supported me all the time. I would also like to my brother and sister for their concern and understanding.

Cheng Ping Lin

July, 2013